FRERES MENTOURI UNIVERSITY
CONSTANTINE 1 -ALGERIA

Journal of Sciences & Technology

Semestrial Journal of Freres Mentouri University, Constantine, Algeria

VOLUME 05 - ISSUE 01— JUNE 2020

EISSN: ….-….

Freres Mentouri
University Constantine

Ain El-Bey Road
Constantine 25000
Algeria

Phone.Fax: 213 (0) 31. 81. 12.78
Email: revues@umc.edu.dz
Website :http://revue.umc.edu.dz

Journal of Sciences & Technology

Volume 5 N° 1 June 2020

Semestrial Journal of Freres Mentouri University
Constantine, Algeria

An article proposed for publication should not be submitted at the same time to another journal.

Manuscripts (original and two copies) should be sent to the following address:

Vice-Rectorate in charge of Post-Graduation and Scientific Research

Direction of Publications and Scientific Animation (15th floor)

Constantine 1 University , Aïn-El-Bey Road, 25000 Constantine, ALGERIA.

Tél./Fax: 213 (0) 31.81.12.78

e-mail: revues@umc.edu.dz

Journal of Sciences & Technology
Volume 5 N° 1 – June 2020

SCIENTIFIC COMMITTEE

INSTRUCTIONS TO AUTHORS

I- Overview

The journal Human Sciences publishes in three languages: Arabic, French and English. Two abstracts must be provided, one in the language of the article, the other in Arabic if the article is written in another language, or in French (or English) if the article is written in Arabic. Abstracts must not exceed 150 words. Unpublished articles are not returned to their authors.

II- Manuscrips

The articles submitted for publication (three copies) must not exceed 20 typewritten pages (tables, figures, graphs, bibliography, ... included) with a large margin to the left (3 cm), printed on 21 x 29 paper , 7 cm (A4) with interligne of good readability. Some flexibility is allowed to authors, but they should organize the text clearly in sections such as: Introduction, Experimental Details, Results, Discussion and Conclusion. The longer articles will be published by part in successive issues, each part being determined by the authors. Authors are kindly requested to accompany the summary of their articles with the most complete possible keywords.

In order to save time and respect deadlines for publication, it is recommended that authors take care of the complete capture of their article on a computer, and send it to the journal, after they have been informed. acceptance for publication, in the form of files on CD.ROM, which will be copied by the service.

However, since the final formatting of the article is done by P.A.O. (Computer Aided Publication), the authors are asked to avoid any formatting of their text. It will be necessary to avoid stylizing it.

III- Bibliography

The bibliographic references quoted in the text must include only the reference number in square brackets (ex .: [5]). If the name of the author appears in the text, it must be followed by the reference number. When the reference contains more than two authors, only the first is cited, followed by "and al".

For articles, the complete reference includes the names of the authors followed by the initials of their first names, the title of the article, the title of the periodical (in conformity with the abbreviations allowed), the volume, the number of the periodical, the year of publication and the relevant pages.

For the works, the reference must include the names of the authors followed by the initials of their first names, the complete title of the work, the volume, the volume, the first and the last page relating to the results discussed, the number of the edition if there are several, the name of the publisher, the place and the year of edition.

For scientific meetings (congresses, proceedings, ...), the reference includes the names of the authors followed by the initials of their first names, the title of the communication, the identification of the meeting, the place, the period and the pages concerned.

IV- Iconography

Tables, boards, charts, maps, photographs, etc. must be provided separately, inset. They must be presented on white sheets of A4 format, individually or in groups, and have underneath the words "table" or "figure" assigned a number.

The illustrations and figures must be clear, professionally made and adequate for reproduction: a 50% reduction, if any, must lead to a suitable size and thickness of characters for good readability. Moreover, for computer-generated figures, in order to maximize contrast, the use of a laser or inkjet printer is essential.

Legends assigned their numbers must be grouped in a separate page.

The final presentation of the article will be left to the discretion of the Editorial Board.

SUMMARY

SUMMARY

COMPARATIVE STUDY BETWEEN THE EFFECT OF TRICHODERMA VIRIDE AND DIFENOCONAZOLE TO INHIBIT GROWTH MYCELIAL Of FUSARIUM OXYSPORUM

Submited on 21/10/2019 – Accepted on 03/06/2020

Abstract

Direct confrontation tests between T. viride and F. oxysporum on agar medium (PDA) revealed considerable activity by the biocontrol agent on the pathogen. After six days of incubation, the average diameter of the pathogen colony was 26 mm and the percent of inhibition was 63.83% relative to the control with 71 mm. At the end of the eighth day, T. viride completely invades the F. oxysporum colony and sporulates on it.The results of the test fungicide revealedmoderate inhibition of mycelial growth of the pathogen, so the concentration of 300 ppm was considered a threshold of inhibition of mycelial growth of F. oxysporum, which appeared sensitive.Otherwise, F.oxysporum appeared resistant against the different concentrations (30 and 3) ppm of Difenoconazole.According to literature and several studies carried out in this field, it has been concluded that T. viride is very effective against pathogenicity of F.oxysporum, whereas the use of fungicide (Difenoconazole) is effective but with varying degrees.

Keywords **:** T.viride, F.oxysporum, Difenoconazole, activity, comparative.

ZEHAIRA BOUZIANE [1]

LAID DEHIMAT [2]

1 Department of Environmental Science and Agricultural Science, University Mohamed Seddik Benyahia- Jijel, Algeria.

2 Department of Applied Biology, Frères Mentouri University Constantine, Algeria.

zh_bouziane@yahoo.fr

INTRODUCTION

Fungicides are products that kill or inhibit the fungi that cause certain diseases. Such as fungal diseases that cause severe damage to cultivated plants [1].With the pesticides, human have been able to control their food crops, escaping the spread of many pests. Fungicides based on copper Sulphate are spreading, especially the famous bordeaux mixture (a mixture of copper sulphate and lime) to fight fungal outbreaks of potatoes. Mercury salts are used at the beginning of the 20th century for the treatment of seeds. The Benzimidazole and Pyrimide fungicides date back to 1966, followed by the Imidazole and Triazolic fungicides known as the Sterol synthesis inhibitor (IBS) fungicide [2] .

After the adverse effects of the use of chemicals on the environment (appearance of resistant strains and accumulation of fungicide residues), control of plant infections caused by fungal pathogens is also considered more frequently by a biological approach [3]. Interest in biological control has greatly increased in recent years.

*Trichoderma*species have received considerable attention as a biological control agent against a number of soil-borne pathogens. Research on mechanisms to control pathogenic populations in the rhizosphere suggests that the antagonistic activity of *Trichodermasp* lies in the production of extracellular enzymes and / or antibiotic substances [4].

The aime of study is to determine the inhibitory capacity of *T.viridein -vitro* against a telluric fungi*F.oxysporum*. We therefore found that this agent plays a very important role in the inhibition of the development of the pathogen, either in direct contact or in distance, which will allow the future to use it *in- vivo*, then to suppress the proliferation of pathogens.

MATERIAL AND METHODS

1. Biological material

1.1. The antagonist agent

The biocontrol fungus used in this study is *T. viride*, it has been isolated from the soil of the Jijel region where it has grown the maize plant.

The identification of the biological control agent was carried out based on morphological characters (macroscopic and microscopic study), the identification is carried out in the Laboratory of Mycology, Biotechnology and Microbial Activity, Department of Microbiology and Biochemistry, University Mentouri Constantine1 Algeria.

1.2. The pathogen agent

The isolate of *Fusariumoxysporum*used in this study was obtained from palm leaves grown in Oumech commune (Biskra).Algeria. The pathogen is identified in laboratory of microbiology. Department of Environmental Sciences and Agronomic Sciences. University Jijel.

1.3. The fungicide

The fungicide used is Dividend®, it applies on seed and the grains, used against pests, charcoal, square and *Septoria*, it is in soluble form (Table1).

Table1: Fungicide information

Trade Name	Active ingredient	Approved dose	Used
Dividend®	Difenoconazole 30g / l	20 ml / KMTL seed	Treatment of seeds against pests, charcoal, *Fusarium*, *Septoria*

METHODOLOGY

1. Antagonist activity of *Trichodermaviride* against *Fusariumoxysporum*

The confrontation test between *T. viride* and the *F.oxysporum* strain was carried out in Petri dishes containing the medium (PDA), two mycelial disks 5 mm in diametre (the first containing *T. viride* and the other carrying *F.oxysporum*) are placed diametrically on the culture medium.

Incubation is carried out at 25 ° C for six days. Notations concerning the inhibition of diametral growth of *Fusariumoxysporum* colonies and their invasion by *T. viride*mycelial were performed daily. The control contains only the pathogen (*Fusariumoxysporum*) in the center of the Petri dish containing the medium (PDA).

The evaluation of the inhibition exerted by the antagonist agent (*T.viride*) is estimated by calculating the percentage inhibition of mycelial growth according to the following formula [5; [6].

$I\% = (1-Cn/Co)\times 100$

Or:

I (%): percentage inhibition of mycelial growth.

Cn: the average diameter of the colonies in the presence of the antagonist.

Co: the average diameter of control colonies.

2. Fungicidal-pathogenic test

The choice of concentrations is making on the basis of preliminary tests and the work of some authors [7] ;[8] .

3. Fungicide test –*Fusariumoxysporum*

The test is performed according to the method [7]. Fungicides suspended in sterile distilled water are diluted to the desired concentrations (3000, 300, 30, 3) ppm. Sterile watman paper disks with 5 mm of diametre are impregnated with 1 ml for each concentration and previously deposited on the PDA agar in Petri dishes. The distance between the pathogen and the soaked discs with fungicide is well defined. The dishes are incubated at a temperature of 25°C for six days. The control consists only of a disk containing the pathogen in the absence of disks soaked with fungicide (Fig 1).

With:

1- Sterile wattman disk soaked with fungicide.

2- Disk carrying *F.oxysporum*.

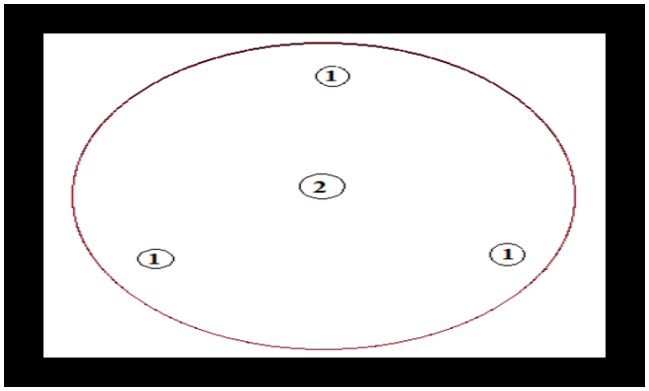

Fig 1. Antagonism test between *F.oysporum* and Difenoconazole on PDA medium at 25°C

RESULTS AND DISCUSSION

The purpose of this study is to test the ability of the antagonist to suppress the growth of the tested pathogen. So, the direct confrontation test shows an inhibitory effect of *Trichodermaviride*against *Fusariumoxysporum*isolate.

1. Direct confrontation on PDA medium between*Trichodermaviride*and *Fusariumoxysporum*

The study of mycelial growth of colony of *Fusariumoxysporum* confronted with *Thrichodermaviride*, shows a significant reduction of the growth of the pathogen compared to the control (Fig2).Simultaneous transplantation of *T.viride* and *F.oxysporum* showed a faster growth of *T. viride* than that of *F. oxysporium* isolate. After 3 days of incubation, *T. viride* invades almost the entire surface of the dish, whereas *F.oxysporum* occupies only 23.5 mm in diametre, and the growth of *F.oxysporum* is stopped during the fourth days with a rate of low growth, which corresponds to the percentage inhibition of mycelial growth with 63.83% (Fig3) (Table 2).According to [5], this interpretation is due to the action of the enzymes (β1-3) gluconase-chitinase which leads to lysis of parasite mycelial.

Table 2: The average diameter of colonies (mm) of *F. oxysporum* in the presence of *T.viride* compared to the control

Colonies / Days	Average diameter of *F.oxysporum* colony	Average diameter of control	Percentage of inhibition %
1	13.5	15.5	12.90
2	21	24	12.5
3	23.5	39	39.74
4	26	55	52.72
5	26	65	60
6	26	71	63.83

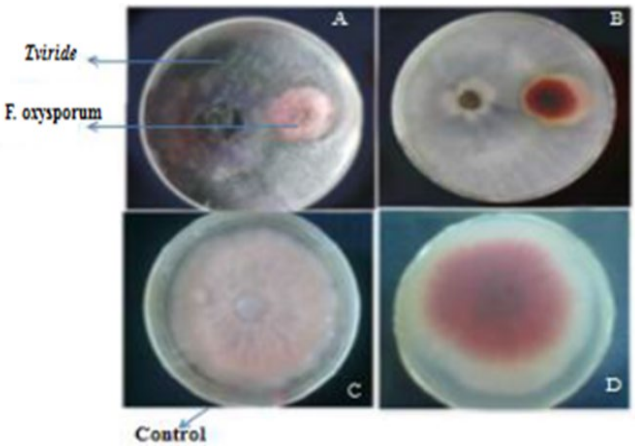

Fig 2. Inhibitory effect of mycelial growth of *F. oxysporum* in the presence of *T. viride* after 72h of incubation at 25 ° C (A (recto): confrontation test, B (verso); C (recto): control colony; D (verso)

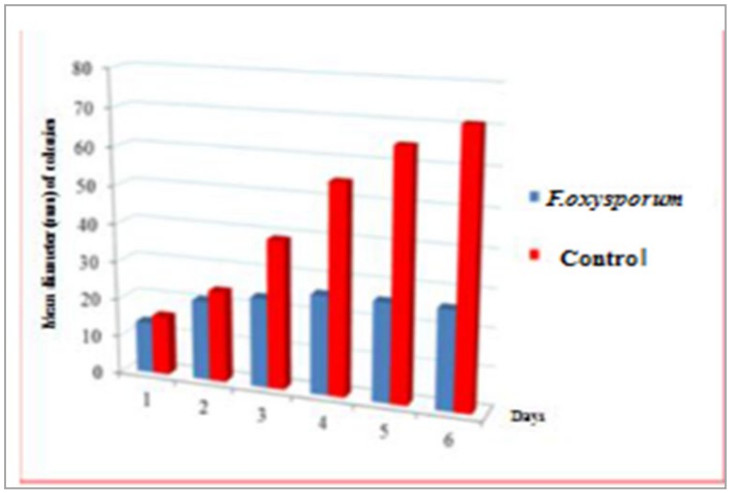

Fig 3. Comparison between the mycelial development of *F.oxysporum* in the presence of *T.viride* and the untreated control

In addition, *Trichoderma* is a fungi that naturally colonises plant soils and roots before phytopathogens, and may play a predominant role in plant health [9]. Various researchers have reported the antagonistic activity of different Trichoderma isolates against phytopathogenic fungi such as *R. solani*, *F. oxysporum* and *Sclerotiumrolfsii* [10].

Control grown alone occupies a surface of 71 mm in diameter after 6 days of incubation; with a light pink aerial mycelial in the early days of its development; then takes a pink-vermilion colour.

After ten days of incubation, it was found that *T.viride*sporulates on the *F.oxysporum* colony, and appears granulose on the surface of the pathogen colony (Fig4).The same results reveled by Otherwise, [11] found that the strain of *T.viride* has an important activity of secreting enzymes in order to attack or suppress the mycotoxinssynthesised by phytopathogens. After six days *T.viride* completely covers the colonies of pathogens on which it sporulates, *T.viride* showed an antagonistic power, which is the ability to stop or suppress the development of pathogens *Verticilliumsp* and *Phoma sp4* [12].[13] observed the invasion of the pathogen colony by *Trichodermaharzianum*, *in- vitro* between this antagonist and *Sclerotinasclerotinium*; [14] conducted a direct confrontation between *Trichodermaharzianum* and a telluric fungus, *F.oxysporum* on medium (PDA).

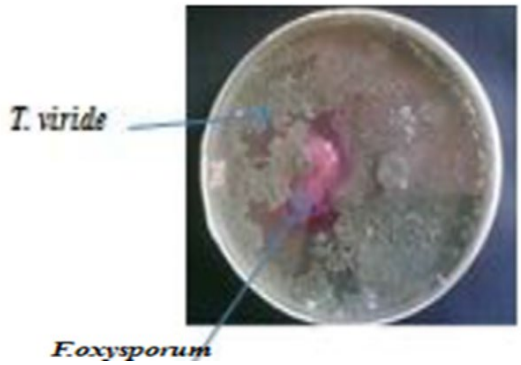

Fig 4. Sporulation of *T.viride* on the *F.oxysporum* after ten days of incubation at 25ºC on PDA medium

2. Fungicide test- *Fusariumoxysporum*

The reduction of mycelial growth is low to medium for the different concentrations of the fungicide (Fig5). The inhibition percentages vary between (16.40 and 64.95) %. After four days of incubation, the mycelial growth of *F. oxysporum* was stopped after treatment with 3000 ppm and 300 ppm, and reached an average diametre of 18.5 mm and 27 mm respectively, whereas, inhibition of mycelial growth of *F. oxysporum* reached 42 mm and 51 mm after five days of incubation, and after treatment with 30 ppm and 3 ppm respectively (Fig6).The concentration required to inhibit 50% of *F.oxysporum*mycelial growth is the 300 ppm of the fungicide used (Table 3).The control of *F.oxysporium* grown alone occupies a surface of 79 mm in diametre after six days of incubation[15]. In addition, [16] showed that systemic fungicides such as Triazoles and Difenoconazole are effective against several cereal diseases. The use of pesticides helps prevent the spread of certain diseases, such as the mildew, transmitted by parasitic fungi.

Total inhibition was observed for the isolate tested at 3000 ppm Difenoconazole. There are also variable responses of the isolate to other concentrations. Where 50% inhibition of mycelial growth of *F.oxysporum* is recorded at 300 ppm compared to the control. This raises the problem of resistance to fungicides and the proliferation of the pathogen in a normal way. Fungicides are one of the means of fight against phytopathogenic fungi and must contribute.Pesticides have a negative impact on ecosystems (water pollution, poisoning of bees, birds or earthworms, etc.). Many of these pesticides are toxic to living organisms. A chemical that kills a fly can also kill a dog. The repetitive use of the same product and sometimes misguided pesticides gives rise to insects, plant diseases, weeds resistant to some of these products [17].

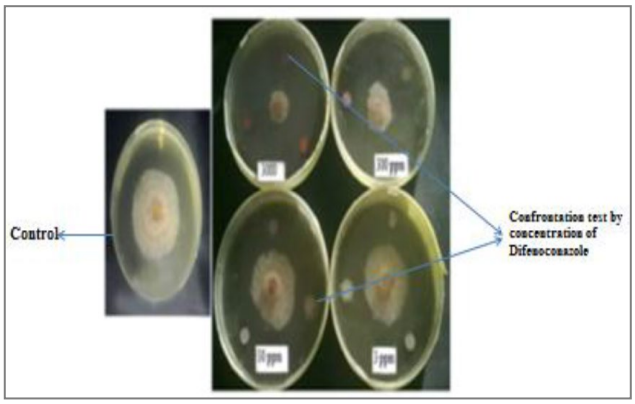

Fig 5.Effect of different concentrations of the fungicide on the mycelial growth of *Fusariumoxysporum* after four days of incubation at 25ºC

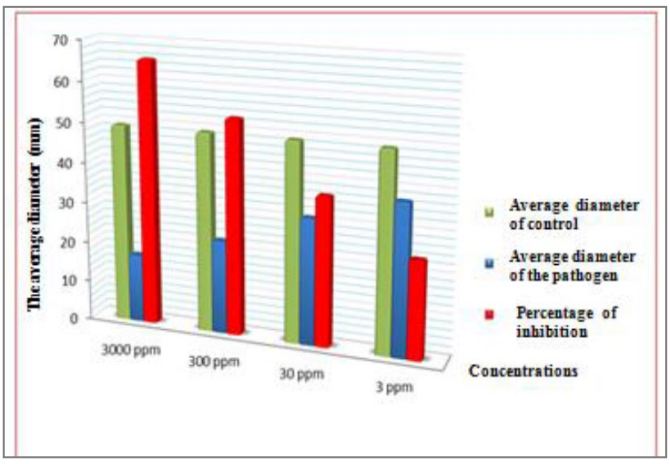

Fig 6. Average diameter of colonies (mm) of *F.oxysporum* treated with the fungicide (deferent concentrations) and inhibition rate after six days of incubation

Table 3:Average diameter of colonies (mm) of *F. oxysporum* treated with the fungicide (different concentrations) and inhibition rate after six days of incubation

Difénoconazole (ppm)	First day	Second days	Third days	Fourth days	Fifth days	Sixth days	Average diameter (mm) of colonies	Percentage of inhibition
3000	13.5	15	17.5	18.5	18.5	18.5	16.91	64.95
Control1	14	23	45	61	69	77.5	48.25	
300	14	20	23.5	27	27	27	23.08	52.65
Control 2	14.5	23	44	63	70	78	48.75	
30	14	23	31	41	42	42	31.16	35.19
Control 3	14.5	25	42	61	69	77	48.08	
3	14	24.5	35	49	51	51	37.41	16.40
Control 4	14	24	43.5	64	71	79	44.75	

Pesticides protect plants or plant products against all pests or prevent their action, and destroyed the undesirables. In addition, many pesticides are toxic, therefore dangerous for human health (congenital malformations, cancers, neurological disorders, fertility and immune system).

CONCLUSION

This work has two parts: biological control and chemical control. The first part is devoted to the study of the effect of biocontrol fungi using *T.viride* against *F.oxysporum*.The effect of *T.viride* is manifested by an inhibitory activity of mycelial growth of *F.oxysporum* with a percentage inhibition that reaches 63.83%.The second part consists of an *in- vitro* test using Difenoconazole (chemical control) against the *F.oxysporum* isolate. It has been shown that the 300 ppm concentration shows a 50% reduction in mycelial growth, so the tested isolate is more susceptible to fungicide.

According to this study, *T. viride* has been shown to play a very important role in biological control, while the use of Difenoconazole fungicide with respect to *F. oxysporum* shows a variability of inhibitory action according to the concentration (300 ppm).

PERSPECTIVE

The realisation of this study has enriched our knowledge of biological and chemical control; and we can afford to fix these points as perspectives.

- The application of *in- vitro* tests perform by *in- vivo* tests.

- The widening of the range of the studied species in order to deepen the results and to understand the interactions between the species.

-Study the side effects of chemical control on the environment and human health.

-The application of *in- vivo* tests in natural conditions.

REFERENCES

[1]-C. Garon-Boucher, and C. Margoum, Contribution to the study of the fate of phytosanitary products during runoff in pits. Physicochemical and hydrodynamic characterisation.(Université Joseph Fourier-Grenoble I, France), 2003.P 244.

[2]-G. Tawil, Bibliographic study on the effect of pesticides on human health, Master 2 Research "Development of quality and food safety", (National Veterinary School, Toulouse, 17- France), 2007.P 14.

[3]-C. Rafin, and Y. Tirilly, Characteristics and pathogenicity of *Pythiumsp* associated with rot of tomatoes in soil culture in Brittany, France. Plant Pathol, Vol 44. 1995. 779 - 785.

[4]-Y. Elad, and A. kapar, The role of *Trichodermaharzianum* protease in the biocontrol of *Botrytis cinerea*. Eur J Plant PatholVol 105. 1999. 177 - 189.

[5]-P. Comporta, In- vitro Antagonism of *Trichodermaspp* against *Rhizoctoniasolanikühn*. Agronomies Vol 7. 1985. 613 - 620.

[6]-A. Hmouni, MR. Hajlaoui, and A. Mlaiki, Resistance of *Botrytis cinérea* to Benzimidazoles and Dicarboxamides in sheltered tomato crops in Tunisia. OEPP/EPPO bull.Vol 26. 1996. 697-705.

[7]-ZN. Wang, JR. Coley smith JR, and PW. Wareing, (Dicarboxamides resistance in *Botrytis cinerea* in protected lettue-Plant Pathol, Vol 35(4). 1986. 427- 433.

[8]-T. Hseiang, and GA. Chastagner, Grow and virulence of fungicide resistant field isolates of three species of *Botrytis cinerea-Can. J. Plant Pathol.* Vol**13(3**). 1991. 226-231.

[9]-W. Gams, andJ. Bisset, Morphology and identification of *Trichoderm*a. In: Kubicekcp, Harman GE (Eds*Trichoderma* and *Gliocladium*, *vol1Taylor and Francis*. London UK. 1998.P3-33.

[10]-T. EslaminejadParizi, A. Mehdi, and T. Eslaminejad, Evaluation of the potential of *Trichodermaviride* in the control of fungal pathogens of Roselle (Hibiscus sabdariffa L) in- vitro. Microbial Pathogenesis.Vol 52. 2012. 201-205.

[11]-E. Pates, F. Meredith, W. Smart, CW. Bacon, and AJ. Jaworski, *Trichodermaviride* suppresses de fumonisin B1 production by *Fusariummoniliforme* J. Food Protects, Vol 66. 1999. 1326 -332.

[12]-Z. Bouziane, L. Dehimat, W. Abdelaziz, and N. Kacemchaouche, (2011).The competition of *Trichodermaviride* opposite fungal pathogenic strains of *Zea mays* plant.(Laboratory of Applied Mycology.Université des Frères Mentouri- Constantine1). Sciences&TechnologieC –N°33Juin(2011), pp.31-37.

[13]-MA. Cundon, M. Mazzanti, S. Castanon, and SA. Gutiérrez, Actividadantagoniticai*n- vitro* deaislamientos de *Trichodermaharzianum*, sobreexlerocios de *Sclerotiniasclerotinium*. Communication Cientificas y Tecnologicas.(Universitad National Del Nordeste, Facultad de CienciasAgrarias-UNNE.Sargentocabral, corrientes, Argentina), 2000.

[14]-N. Benhamou, P. Rey, M. Cherif, J. Hockenhull, and Y.Tirilly, Treatment with the mycoparasite*Pythiumoligandrum* triggers induction of defence-related reactions in tomato roots when challenged with *Fusariumoxysporum f. sp*. radicis-lycopersici. Phytopathology Vol 87. 1997. 108-121

[15]-P. Leroux, Modes of action of plant protection products on plant pathogenic organisms .CR Biologies, Vol 326. 2003b. 9 -21.

[16]-RA. Martin, and JB. Sanderson, Yield of barley in response to Propiconazole. - Can. J. Plant Pathol, Vol 10(1). 1988. 66 -72.

[17]-P. Leroux, General report on chemical control of phytopathogenic fungi. Mode of action of fungicides and phenomena of resistance. - 4th Congress on the Protection of Human Health and Crops in a Tropical Environment, (Marseilles Chamber of Commerce and Industry, France), 1986. P148-162.

Sciences & Technology **Vol 5 – N°1**, June 2020, pp. 15-28

EFFECTS OF INCLINED MAGNETIC FIELD AND SLIP BOUNDARY CONDITION ON HEAT AND MASS TRANSFER IN A CASSON NANOFLUID FLOW OVER A STRETCHING SHEET

Submited on 09/01/2020 – Accepted on 14/06/2020

Abstract

In this paper, the effects of inclined magnetic field and slip boundary condition on heat and mass transfer in a Cassonnanofluid over a stretching sheet is examined. Brownian motion and thermophoreiss with chemical reation were considered as a nanofluid model and the fluid is electrically conducting in the presence of applied an inclined magnetic field. The nonlinear partial differential equations are transformed to nonlinear ordinary differential equationsby using appropriate transformation, which is solved numerically using a spectral collocation method. The effects of some fluid parameters on velocity, temperature and nanoparticle concentration profiles are shown graphically. Enhancement of both temperature and nanoparticle concentration were observed when there is an increase in thermophoresis parameter N_t and the increase in slip parameter result to decrease in the velocity of the fluid.Local skin friction coefficient, local Nusselt number, and Sherwood number are analysed through tabulated results in table 1and 2.

Keywords: Casson nanofluid, stretching sheet, Inclined Magnetic field, Chemical reaction.

T.W AKAJE *[1]

B.I OLAJUWON [2]

Department of Mathematics, Federal University of Agriculture, Abeokuta, Nigeria.

* akajewasiu@gmail.com

INTRODUCTION

Today nanofluids are gaining more attention of many researchers because of their potential to provide enhanced performance properties, particularly with respect to heat transfer than base fluids. Choi [1] was the first author to introduce the concept of nanofluids where he proposed the suspension of nanoparticles. The suspensions of particles such as metals, metal oxides, carbides, nitrides, carbon, nanotubes etc. dispersed in base fluids such as water, ethylene glycol, refrigerants and engine oil of size less than 100nm are known as nanofluids.

Heat transfer, especially the cooling of microsystems with very large heat fluxes is the major potential application of nanofluids. This has been a focus of many researchers, where microchannel heat sinks were introduced as heat removal devices. Kandikar and Salman [2] studied the convection heat transfer in microchannels using conventional fluids like water and ethylene glycol. Provided that all systems components are carefully designed, nanofluids make a better performance for heat transfer in microchannels than base fluids. Energy loss in mechanical systems is caused majorly by friction, and this can be controlled by providing necessary lubrication to improve the efficiency of energy utilization and the reliability of mechanical systems, and this can be done by adding nanoparticles to the lubricants to enhance their tribological properties, especially in the boundary and mixed lubrication regimes.Hu et al [3] Reported, anti-friction and wear behaviours of a variety of nanoparticles used as lubricants additives, including metals and non-metals.Mustafa and Hayat [4] Discussed unsteady boundary layer flow of nano-fluid past an impulsively stretching sheet. They observed that increase in the Brownian motion and thermophoresic effect enhanced the temperature and thermal boundary layer thickness and when the strength of the thermophoresiceffefect is increase, there is enough increase in Nanoparticle concentration and rate of mass transfer at the sheet. Mathematical modelling and Computer Simulations of nanofluid flow with applications to cooling and lubrication was examined byClement and Zelin[5] and complex mixture occurred when nanoparticles are added to the base fluid (Water) at lower concentration results to physical phenomenion which have been observed in other suspensions. Analytical and numerical study of buoyancy-driven convection in a vertical enclosure filled with nanofluids has been investigated by Alloui, et al [6].investigation on convective heat transfer and flow features of nanofluids is experimentally studied by Xuan and Li [7]. The flow velocity of the fluid and the volume fraction of the nano particles increased with an increase in convective heat transfer coefficient of the nanofluid and this was bigger than that of base fluid (water) under the same velocity.Some materials display properties of the non-Newtonian fluid, which implies that they do not obey Newton's law of viscosity that's the shear stress is not linearly proportional to the rate of shear strain. Examples of such fluids are muds, tomato, glue, paint, emulsion,and condensed milk. The different models of non-Newtonian fluids base on their diverse flow behaviours have been proposed by many researchers. Casson fluid model is a preferred rheological model for many fluids including blood, honey,and sauce. When the shear stress becomes greater than the yield stress, Casson fluid starts to deform, but behave like solid when the shear stress is less than the

yield stress.In the category of non-Newtonian fluids, the Cassonfluid has distinct features. It has significant applications in polymer processing, industries and biomechanics.Bhattacharyya, [8] examined MHD Stagnation-Point Flow of Casson fluid and heat transfer over a stretching sheet with thermal radiation and the results show that due to thermal radiation, the temperature inside the boundary layer decreases and the velocity boundary layer thickness for Casson fluid is larger than that of a Newtonian fluid. Buoyancy and the chemical reaction effects on MHD Flow of Casson fluids through a porous medium due to a porous shrinking sheet were examined byKhalid et al[9]. The study of thermal Marangoni convection in the two-phase flow of dusty Casson fluid was investigated by Mahanthesha, and Gireesh [10]. Effects of magnetic field in squeezing flow of a Casson fluid between parallel plates analysed byNaveed et al[11] and it noticed that a strong magnetic field can be used to enhance the flow when plates are coming together and squeeze number increases the velocity profile for both the cases, i.e., when plates are coming closer and when plates are going apart.Sathies, and Gangadhar, [12] Studied the effect of chemical reaction on slip flow of MHD Casson fluid over a stretching sheet with heat and mass transfer. It is seen that in all cases the thermal boundary layer is formed and the temperature at a point decreases with, velocity ratio parameter. Analytical solution of MHD stagnation-point flow and heat transfer of Casson fluid over a stretching sheet with partial slip was presented inSamir Kumar[13]. It was noticed that the magnitude of velocity is greater in the case of Casson fluid when compared with the viscous fluid.Waqar et al [14] analysed the flow of Cassonnanofluid with viscous dissipation and convective conditions: A mathematical model. And it was found that a higher value of Casson parameter leads to a decrease in the temperature and nanoparticle concentration while effects of thermophoresis and Brownian motion parameters on nanoparticle concentration are quite opposite. Convective heat transfer and MHD effects on Cassonnanofluid flow over a shrinking sheet investigated byHussain et al[15] and the result show that the temperature profile and concentration profile decreases when both and increases.Rizwan et al[16] Investigated unsteady Cassonnanofluid flow over a stretching sheet with thermal radiation, convective and slip boundary conditions, and the study showed that by increasing the Casson, Dufour,and unsteadiness parameters, reduced the fluid velocity, temperature,and concentration profiles. Oyelakin et al[17] presented Unsteady MHD non-Darcian flow of a Cassonnanofluid between two parallel plates with heat and mass transfer and it was reported that the velocity, temperature and nanoparticles concentration is found to increase monotonously with time and that the velocity reaches the steady-state faster than the temperature and nanoparticles concentration. MHD slip flow and heat transfer of Cassonnanofluid over an exponentially stretching permeable sheet were studied by [18] and it was reported that momentum boundary layer thickness decreased with the increasing magnetic field intensity, also magnetic parameter reduced the skin friction coefficient, heat flux,andmass flux coefficients. [19] Analysed the effect of MHD and porosity on exact solutions and flow of hybrid Cassonnanofluid.

2. MATHEMATICAL FORMULATIONS

Consider the steady two-dimensionalincompressible flow of an electrically conducting and chemically reactive Cassonnanofluid bounded by a stretching sheet at $y = 0$, with the flow being confined in $y > 0. u_w = bx$ is the stretched linear velocity where b is the positive constant. Strength of the inclined magnetic field is B_o, and here $T_\infty and\ C_\infty$ are the ambient temperature and nanoparticle concentration fields with $T_\infty > T_w$. Thermophoresis and Brownian motion of nanoparticles are taken into consideration. The rheological equation of state of an isotropic and incompressible flow of Casson fluid is given by [8]:

$$\tau_{ij} = \begin{cases} \left(\mu_B + \frac{p_y}{\sqrt{2\pi}}\right) 2e_{ij}, & \pi > \pi_c \\ \left(\mu_B + \frac{p_y}{\sqrt{2\pi_c}}\right) 2e_{ij}, & \pi < \pi_c \end{cases} \quad (1)$$

where μ_D is the plastic dynamic viscosity of the non-Newtonian fluid, p_y is the yield stress of fluid, π is the product of the component of deformation rate with itself, namely, $\pi = e_{ij}e_{ij}, e_{ij}$ is the $(i,j)^{th}$component of the deformation rate and πc is the critical value of π based onthe non-Newtonian model.The governing equations of momentum, energy and mass are:

$$\frac{\partial u}{\partial x} + \frac{\partial v}{\partial y} = 0 \quad (2)$$

$$u\frac{\partial u}{\partial x} + v\frac{\partial u}{\partial y} = v\left(1 + \frac{1}{\beta}\right)\frac{\partial^2 u}{\partial y^2} - \frac{\sigma B_o^2}{\rho} u \sin^2\varphi \quad (3)$$

$$u\frac{\partial T}{\partial x} + v\frac{\partial T}{\partial y} = \frac{k}{\rho_{c_p}}\frac{\partial^2 T}{\partial y^2} + \tau\left[D_B\left(\frac{\partial C}{\partial y}\frac{\partial T}{\partial y}\right) + \frac{D_T}{T_\infty}\left(\frac{\partial T}{\partial y}\right)^2\right] + \frac{\mu}{\rho_{c_p}}\left(1 + \frac{1}{\beta}\right)\left(\frac{\partial u}{\partial y}\right)^2 + \frac{\sigma B_o^2}{\rho}u^2\sin^2\varphi + \frac{Q_0(T - T_\infty)}{\rho_{C_p}} \quad (4)$$

$$u\frac{\partial C}{\partial x} + v\frac{\partial C}{\partial y} = D_B\frac{\partial^2 C}{\partial y^2} + \frac{D_T}{T_\infty}\frac{\partial^2 T}{\partial y^2} - K_o(C - C_\infty) \quad (5)$$

With the given boundary conditions:

$$u = u_w + \left(1 + \frac{1}{\beta}\right) N\,\rho v\frac{\partial u}{\partial y},$$

$$v = 0, T = T_w + K_1 \frac{\partial T}{\partial y}, \quad C = C_w + K_2 \frac{\partial C}{\partial y}, \quad at \ y = 0,$$

$$u = 0, \ T = T_\infty, \ C = C_\infty, as \ y \to \infty \quad (6)$$

where u and v are the velocity components in x and y directions respectively, u_x is the linear velocity,$\upsilon$is the kinematic fluid viscosity, ρ is the fluid density, $\beta = \mu_B \sqrt{\frac{2\pi_c}{p_y}}$ is the Cassonparameter,σ is the electrical conductivity of the fluid, T is the temperature, k is the thermal conductivity,c_p is the specific heat,T_w is the constant temperature at the sheet and T_∞ is the free stream temperature assumed to be constant,$\alpha = \frac{K}{\rho_{c_p}}$I s the thermal diffusivity of the base fluid, $\tau = \frac{(\rho c)_p}{(\rho c)_f}$ is the ratio of nanoparticle heat capacity and the base fluid heat capacity, $D_B$is the coefficient of Brownian diffusion, D_T is the coefficient of thermophoretic diffusion, andB_o is the strength of the inclined magnetic field, with the induced magnetic field being neglected.

Consider the following dimensionless transformations

$$\eta = \left(\frac{b}{\upsilon}\right)^{\frac{1}{2}}, \ \psi(x,y) = (b\upsilon)^{1/2} x f(\eta), \quad \theta(\eta) = \frac{T - T_\infty}{T_w - T_\infty}, \phi(\eta) = \frac{C - C_\infty}{C_w - C_\infty} \quad (7)$$

Using the stream function $\psi(x,y)$ such that

$$u = \frac{\partial \psi}{\partial y}, \ v = -\frac{\partial \psi}{\partial x} \quad (8)$$

Therefore, the equation (2) is satisfied.

From the given transformations mentioned above, 3 to 6 become

$$\left(1 + \frac{1}{\beta}\right) f'''(\eta) + f(\eta) f''^{(\eta)} - \left(f'(\eta)\right)^2 - H_a \sin^2 \varphi \, f'(\eta) = 0 \quad (9)$$

$$\frac{1}{Pr} \theta''(\eta) + f\theta' + N_b \phi' \theta' + N_t \theta'^2 + \left(1 + \frac{1}{\beta}\right) E_c f''^2 + H_a E_c \sin^2 \varphi = 0 \quad (10)$$

$$\phi'' + \mathrm{Le} f \phi' + \frac{N_t}{N_b} \theta'' - Le \chi \phi = 0 \quad (11)$$

$$f(0) = 0, \qquad f'(0) = 1 + \lambda \left(1 + \frac{1}{\beta}\right) E_c f''(0),$$

$$\theta(0) = 1 + \gamma \theta'(0), \quad \phi(0) = 1 + \delta \phi'(0)$$

$$f'(\infty) = 0, \ \theta(\infty) = 0, \ \phi(\infty) = 0. \quad (12)$$

Where prime represents differentiation with respect to η, θ is the dimensionless temperature, ϕ is the dimensionless nanoparticle volume fraction, $H_a$is Hartmann number (magnetic parameter), γ is the thermal slip parameter, Le is Lewis number, χ is the chemical reaction parameter, P_r is Prandtl number, λ is the slip parameter, Ec is the Eckert number, δ is the concentration slip parameter, where N_b and N_t represent Brownian motion and thermophoresis parameters respectively.

These are defined as below:

$$Pr = \frac{v}{\alpha}, \qquad Le = \frac{v}{D_B}, \qquad \lambda = N\rho(vb)^{\frac{1}{2}},$$

$$\gamma = K_1 \left(\frac{b}{v}\right)^{\frac{1}{2}}, \qquad \chi = \frac{K_o}{b},$$

$$E_c = \frac{{u^2}_w}{c_p(T_w - T_\infty)}, \qquad \delta = K_2 \left(\frac{b}{v}\right)^{\frac{1}{2}},$$

$$N_b = \frac{(\rho c)_p D_B (C_w - C_\infty)}{(\rho c)_f v},$$

$$N_t = \frac{(\rho c)_p D_T (T_w - T_\infty)}{(\rho c)_f v T_\infty}, \quad H_a = \frac{\sigma {B_o}^2}{\rho b},$$

$$Q = \frac{Q_0}{C\rho_{c_p}} \quad (13)$$

The physical quantities of engineering interest are the Skin friction coefficient (rate of shear stress), the Nusselt number (rate of heat transfer), and the Sherwood number (rate of mass transfer).

The local Skin-friction C_{fx}, local Nusselt Number Nu_x,and local Sherwood Number Sh_x which are defined as

$$C_{fx} = \frac{\tau_w}{\rho {u^2}_w}, \qquad Nu_x = \frac{x q_w}{k(T_w - T_\infty)},$$

$$Sh_x = \frac{x q_m}{D_B (C_w - C_\infty)} \quad (14)$$

Where $\tau_w$is the shear stress, q_w and q_m are the surface heat and mass flux which are given by the following expressions:

$$\tau_w = \left(\mu_B + \frac{p_y}{\sqrt{2\pi_c}}\right)\left(\frac{\partial u}{\partial y}\right)_{y=0}, q_w = -k\left(\frac{\partial T}{\partial y}\right)_{y=0}, q_m = -D_B\left(\frac{\partial C}{\partial y}\right)_{y=0} \quad (15)$$

In terms of dimensionless quantities (14) we have

$$Re_x{}^{1/2}C_f = \left(1 + \frac{1}{\beta}\right)f''(0), \quad \frac{N_u}{Re_x{}^{1/2}} = -\theta'(0), \quad \frac{Sh_x}{Re_x{}^{1/2}} = -\phi'(0), \quad (16)$$

where$Re_x = \frac{xu_w}{v}$ is the local Reynolds number.

3. METHOD OF SOLUTION

The systems of nonlinear differential equations (9-11) parallel to the boundary conditions (12) are solved numerically using the Chebyshevspectralcollocation method. In this method, the unknown functions, $f(\eta), \theta(\eta) and\ \phi(\eta)$ is approximated by the sum of the basic functions $T_n(\eta)$ [20-21]:

$$f(\eta) = \sum_{n=o}^{N} a_n T_n(\eta) \quad (17)$$

$$\theta(\xi) = \sum_{n=0}^{N} b_n T_n(\eta) \quad (18)$$

$$\phi(\eta) = \sum_{n=0}^{N} c_n T_n(\eta) \quad (19)$$

The basis functions are taken as the Chebyshev polynomials, in (17), (18) and (19) which defined in the interval $-1 \le \eta \le 1$ as

$$T_n(\eta) = \cos(N \cos^{-1}\eta) \quad (20)$$

$a_n, b_n and\ c_n$are unknown constant to be obtained. $[o, \infty]$is the considered flow problem domain, which transformed into the $[-1,1]$ of the definition of basis functions, by using the below transformation

$$\eta = \frac{2p}{p_\infty - 1} \quad (21)$$

whereη_∞ denotes the edge of the boundary layer, by substituting (17), (18) and (19) into (9-11), non-zero residual were obtained. The coefficienta_n,$b_n$andc_n were chosen in such a way that the obtained residues minimized throughout the domain.

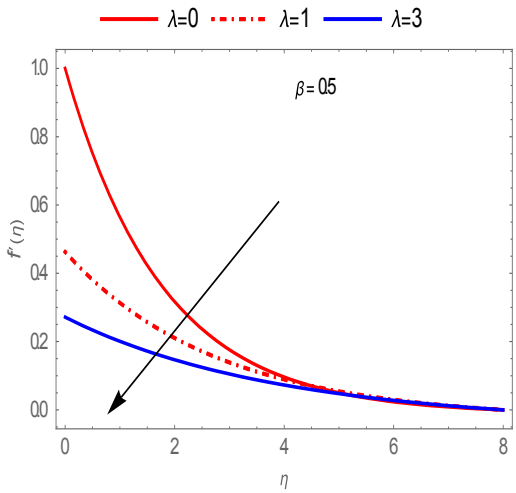

Fig. 1.Behaviour of $\lambda\ on\ f'(\eta)\ for\ \beta = 0.5$

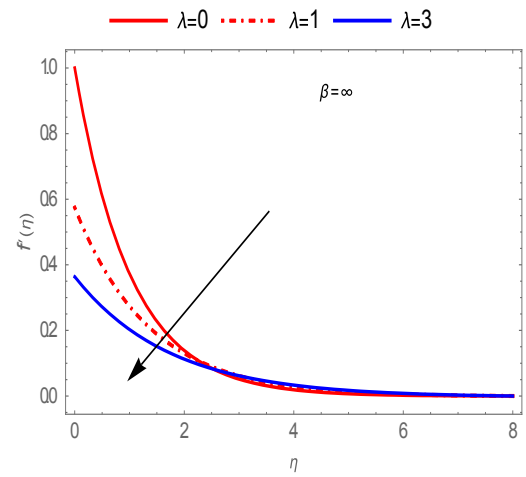

Fig. 2.Behaviour of $\lambda\ on\ f'(\eta)\ for\ \beta = \infty$

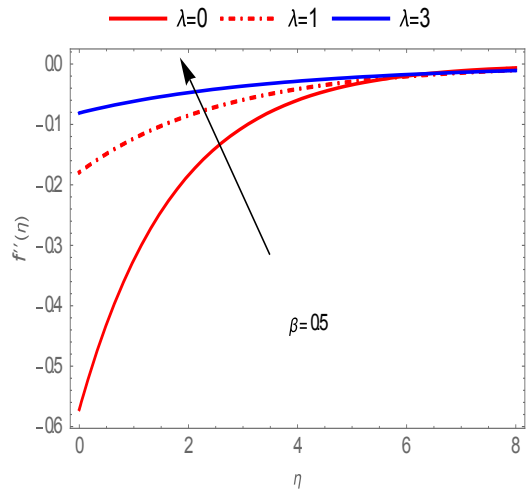

Fig. 3.Behaviour of $\lambda\ on\ f''(\eta)\ for\ \beta = 0.5$

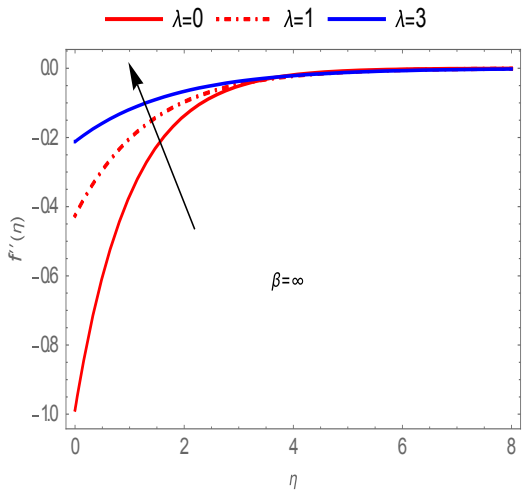

Fig. 4. Behaviour of λ on $f'(\eta)$ for $\beta = \infty$

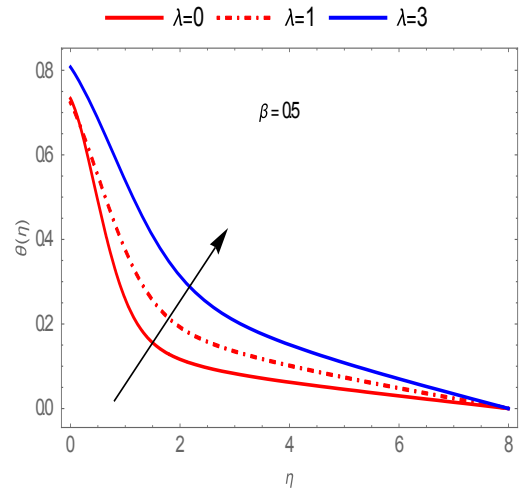

Fig. 5.Behaviour of λ on $\theta(\eta)$ for $\beta = 0.5$

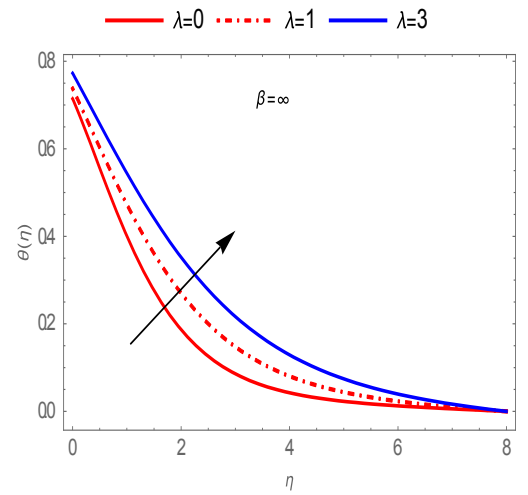

Fig. 6.Behaviour of λ on $\theta(\eta)$ for $\beta = \infty$

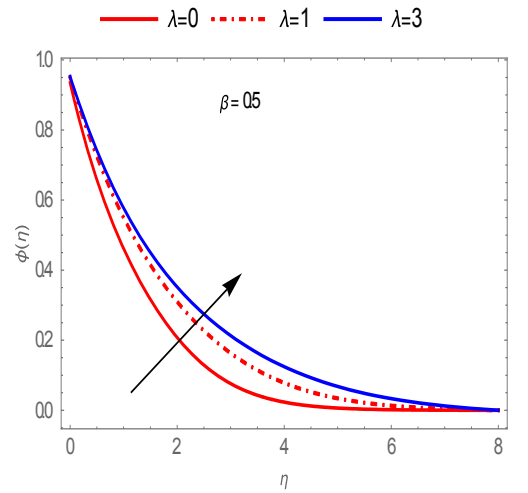

Fig. 7.Behaviour of λ on $\phi(\eta)$ for $\beta = 0.5$

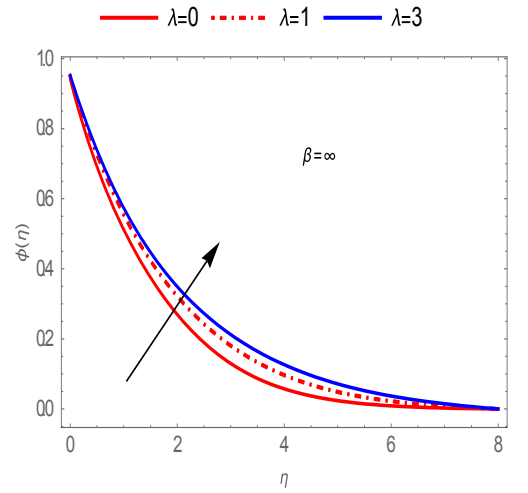

Fig. 8. Behaviour of λ on $\phi(\eta)$ for $\beta = \infty$

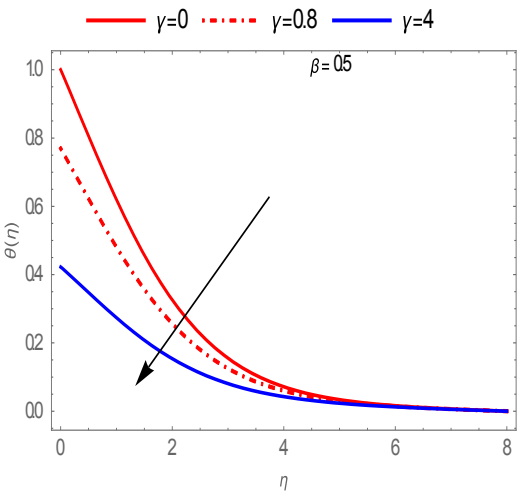

Fig. 9.Behaviour of γ on $\theta(\eta)$ for $\beta = 0.5$

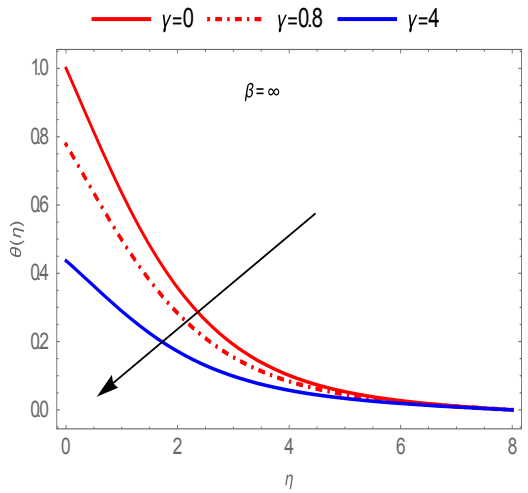

Fig. 10.Behaviour of γ on $\theta(\eta)$ for $\beta = \infty$

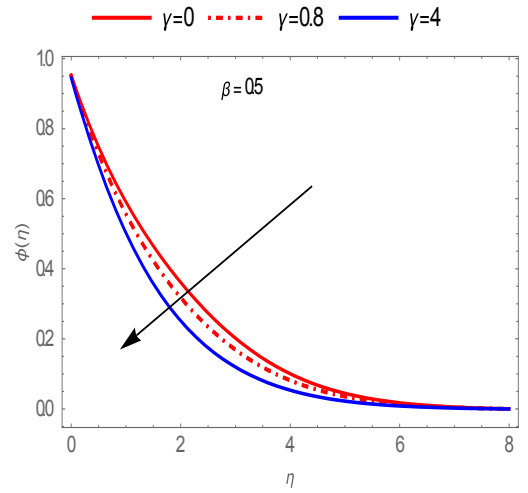

Fig. 11.Behaviour of γ on $\phi(\eta)$ for $\beta = 0.5$

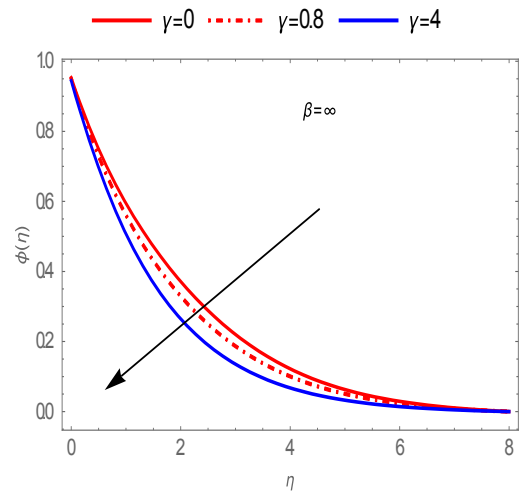

Fig. 12. Behaviour of γ on $\phi(\eta)$ for $\beta = \infty$

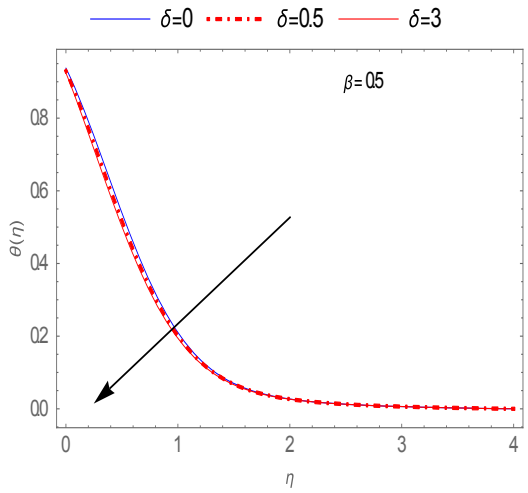

Fig. 13.Behaviour of δ on $\theta(\eta)$ for $\beta = 0.5,$

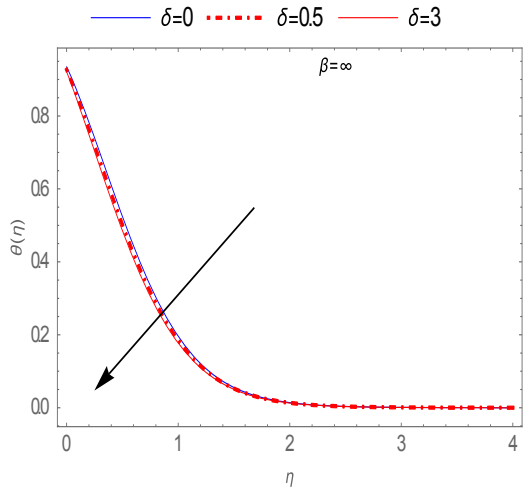

Fig. 14. Behaviour of δ on $\theta(\eta)$ for $\beta = \infty$

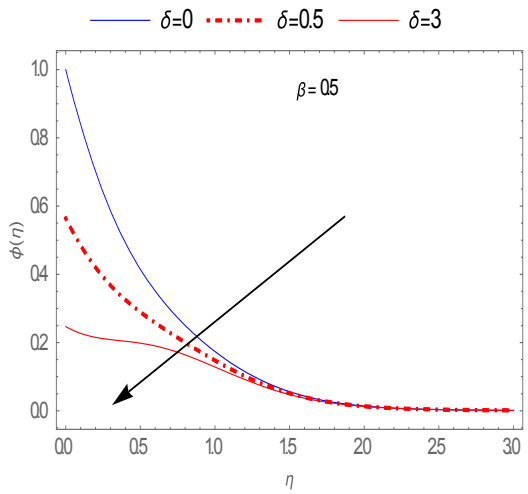

Fig.15. Behaviour of δ on $\phi(\eta)$ for $\beta = 0.5$

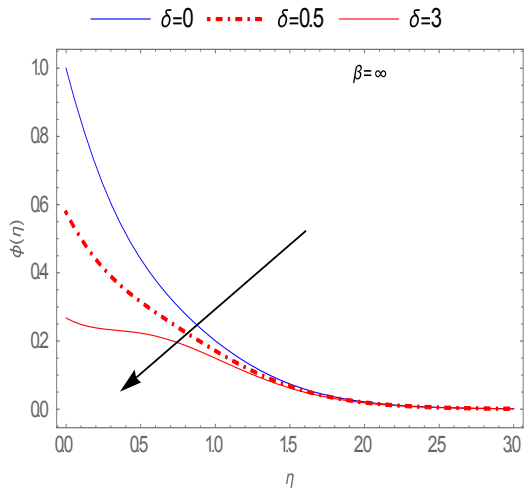

Fig. 16.Behaviour of δ $on \phi(\eta)$ for $\beta = \infty$

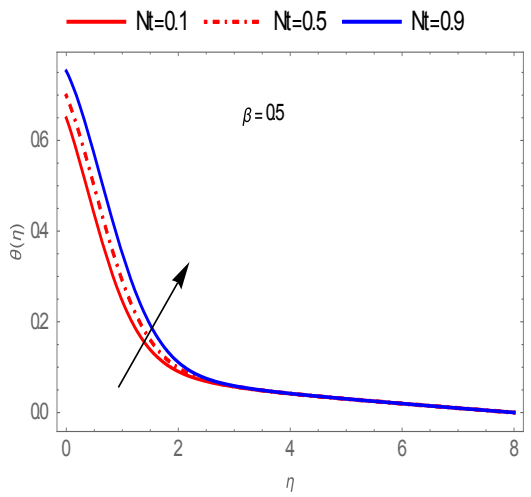

Fig.17.Behaviour of N_t on $\theta(\eta)$ for $\beta = 0.5$

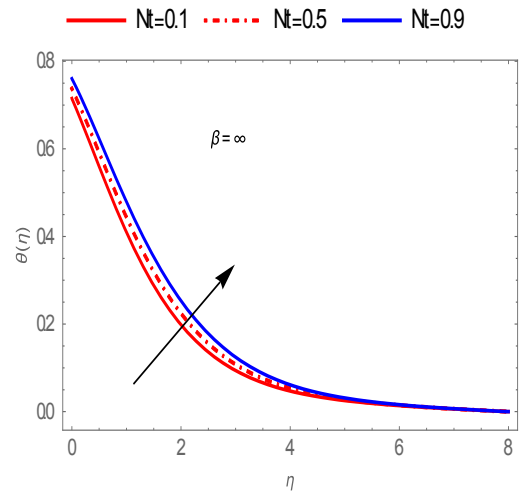

Fig. 18. Behaviour ofN_t on $\theta(\eta)$ for $\beta = \infty$

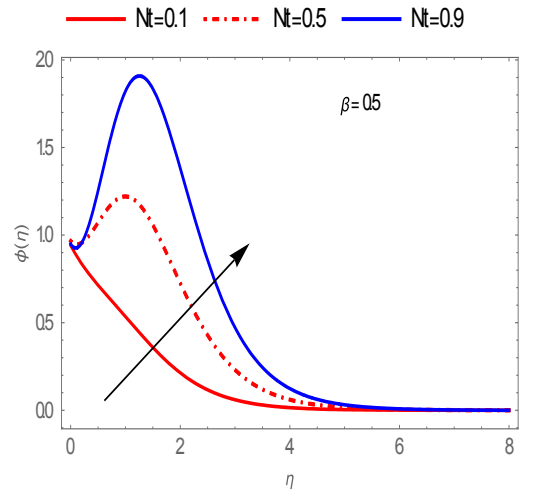

Fig. 19.Behaviour of N_t on $\phi(\eta)$ for $\beta = 0.5$

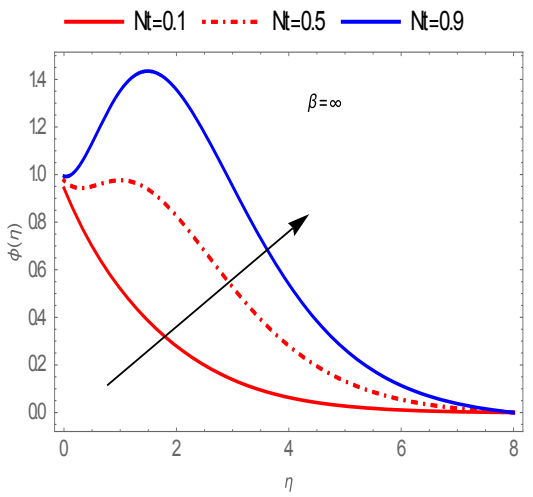

Fig. 20. Behaviour of N_t on $\phi(\eta)$ for $\beta = \infty$

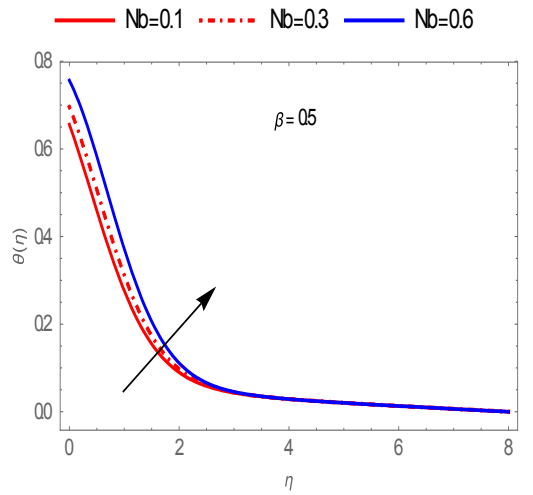

Fig. 21.Bhaviour of N_b on $\theta(\eta)$ for $\beta = 0.5$

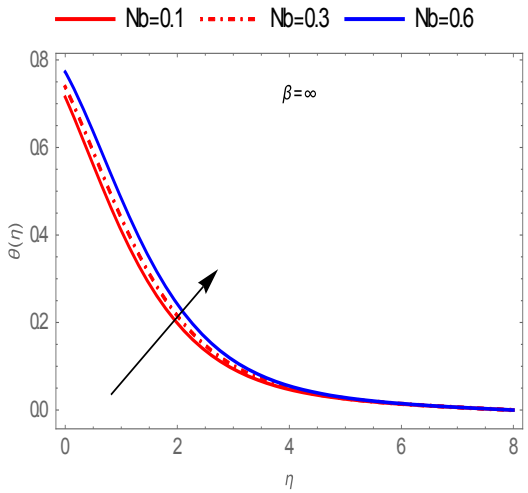

Fig. 22. Behaviour of N_b on $\theta(\eta)$ for $\beta = \infty$

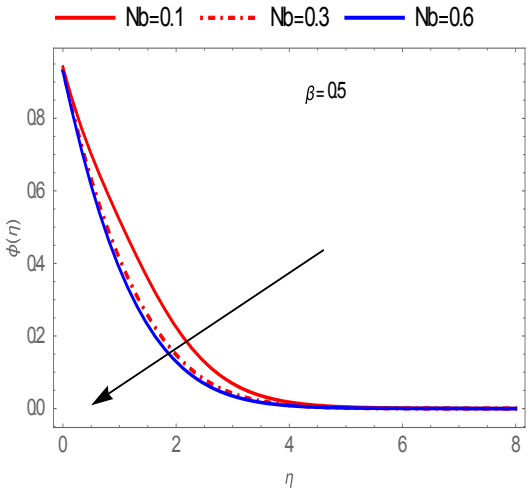

Fig.23.Behaviour of N_b on $\phi(\eta)$ for $\beta = 0.5$

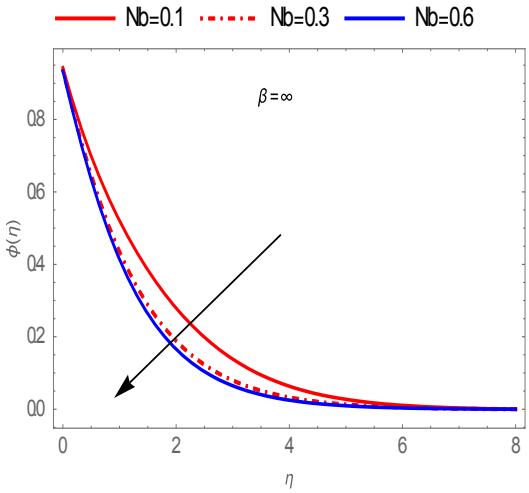

Fig.24. Behaviour of N_b on $\phi(\eta)$ for $\beta = \infty$

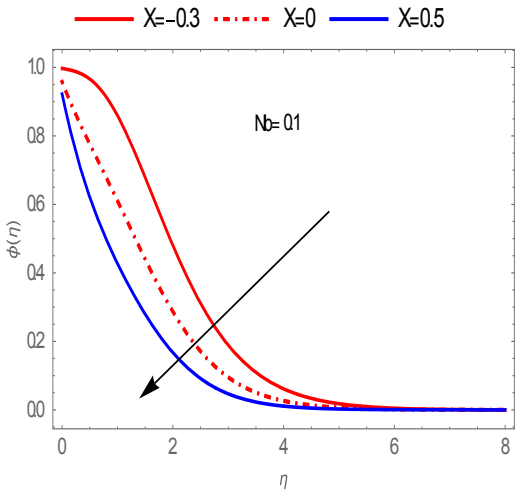

Fig. 25.Behaviour of X on $\phi(\eta)$ for $Nb = 0.1$

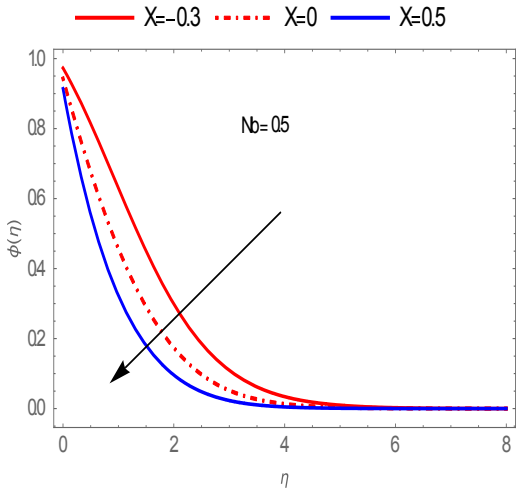

Fig. 26.Behaviour of X on $\phi(\eta)$ for $Nb = 0.5$

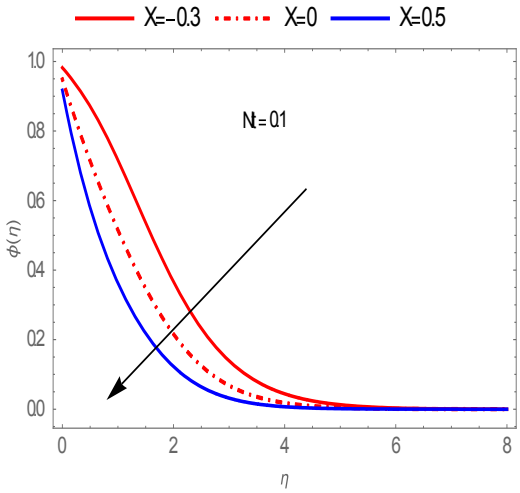

Fig. 27.Behaviour of X on $\phi(\eta)$ for $N_t = 0.1$

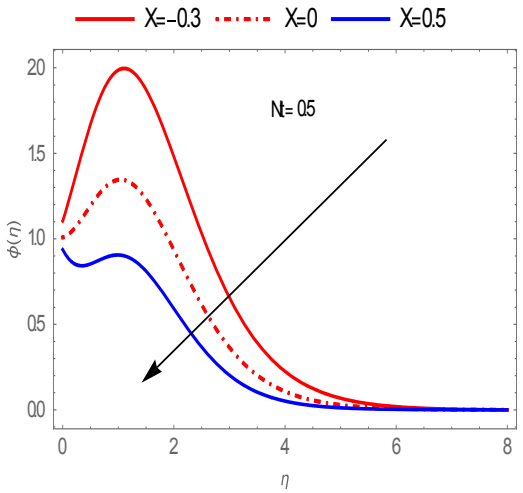

Fig. 28. Behaviour of X on $\phi(\eta)$ for $N_t = 0.5$

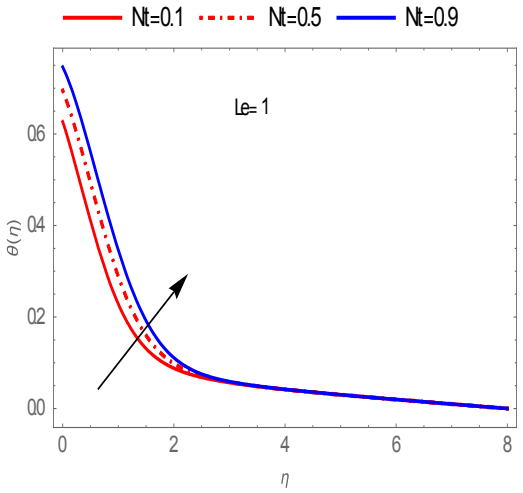

Fig. 29.Behaviour of N_t on $\theta(\eta)$ for $Le = 1$

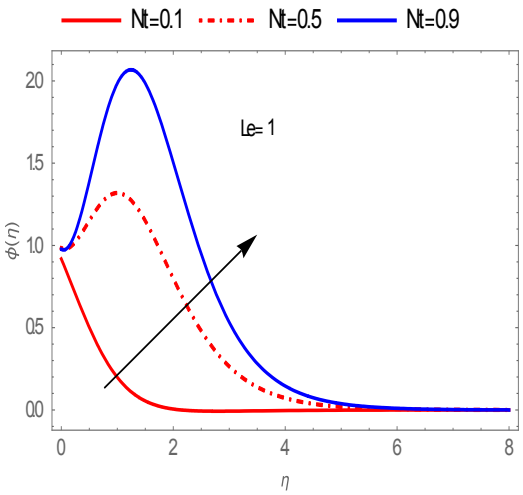

Fig. 30.Behaviour of N_t on $\phi(\eta)$ $Le = 1$

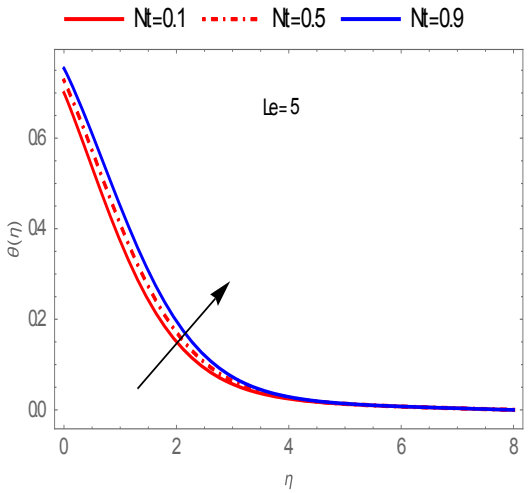

Fig. 31.Behaviour ofN_t on $\theta(\eta)$ for $Le = 5$

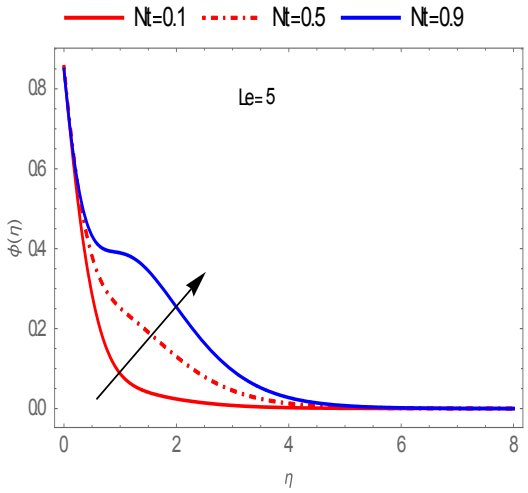

Fig. 32. Behaviour of N_t on $\phi(\eta)$ for $Le = 5$

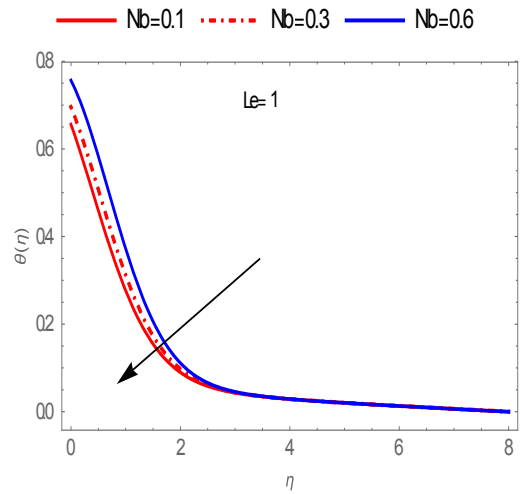

Fig. 33.Behaviour of N_b on $\theta(\eta)$ for $Le = 1$

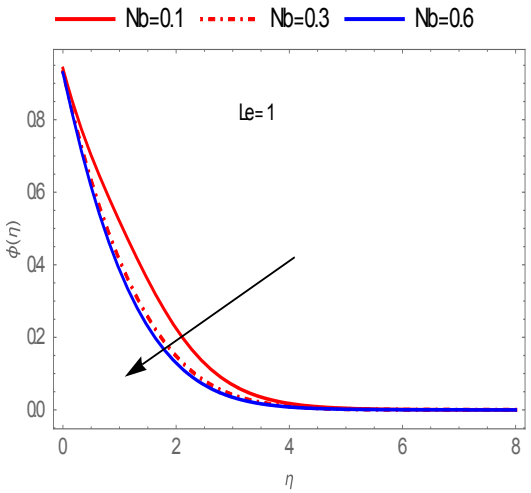

Fig. 34. Behaviour of N_b on $\phi(\eta)$ for $Le = 1$

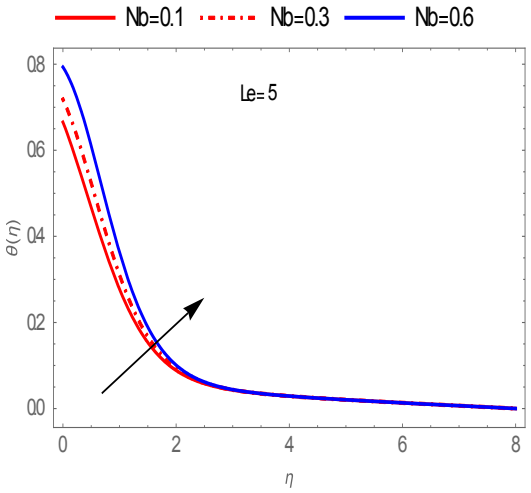

Fig. 35.Behaviour of N_b on $\theta(\eta)$ for $Le = 5$

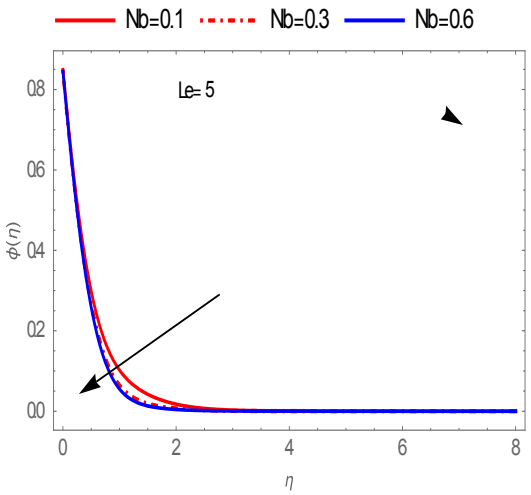

Fig. 36. Behaviour of N_b on $\phi(\eta)$ for $Le = 5$

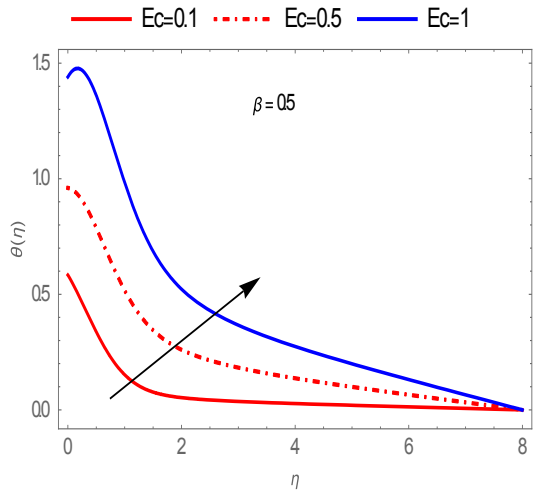

Fig. 37.Behaviour of E_c on $\theta(\eta)$ for $\beta = 0.5$

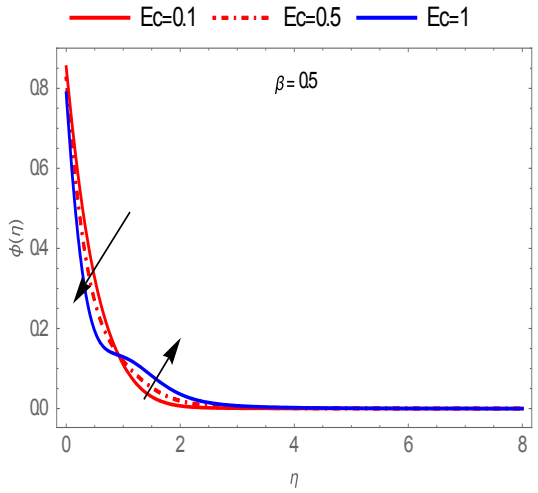

Fig. 38.Behaviour of E_c on $\phi(\eta)$ for $\beta = 0.5$

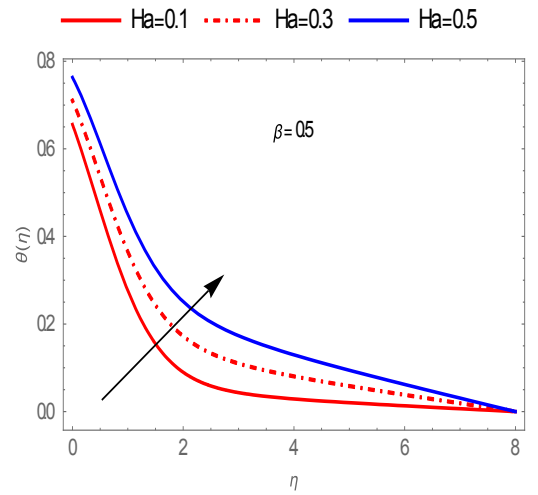

Fig.39.Behaviour of H_a on $\theta(\eta)$ for $\beta = 0.5$

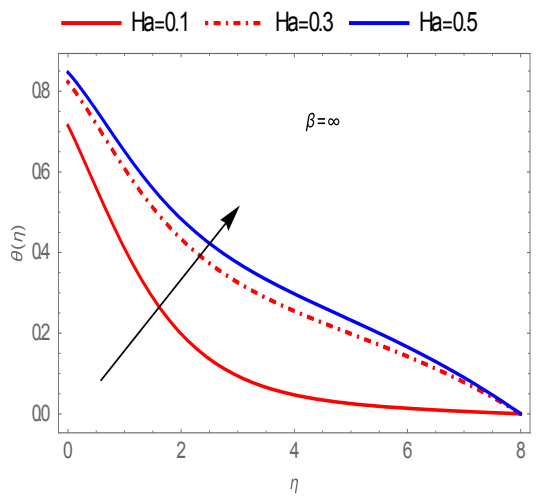

Fig. 40.Behaviour of E_a on $\phi(\eta)$ for $\beta = \infty$

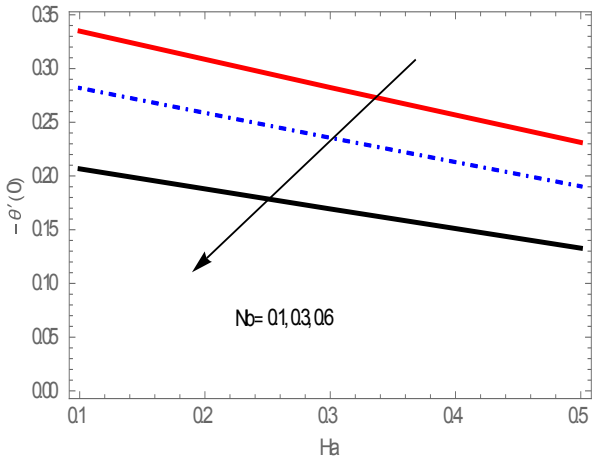

Fig. 41.Behaviour of N_b and H_a $on - \theta'(0)$

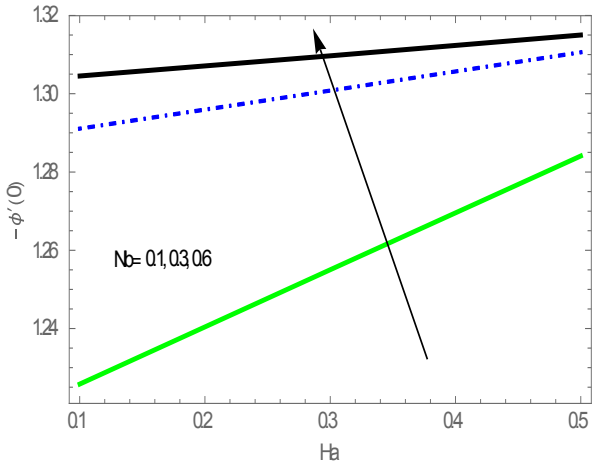

Fig. 42.Behaviour of N_b and H_a $on - \phi'(0)$

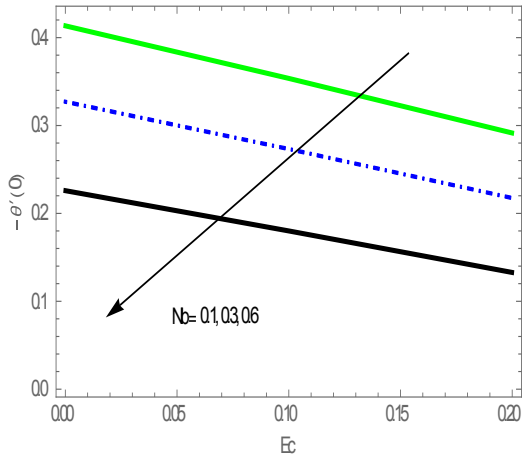

Fig. 43.Behaviour of N_b and E_c on $\theta'(0)$

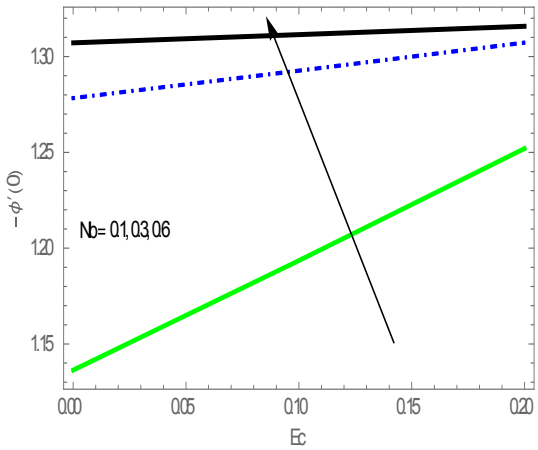

Fig. 44.Behaviour of N_b and Ec on $\phi'(0)$

4. RESULTS ANALYSIS AND DISCUSSION

The nonlinear ordinary differential equations (9) – (11) subjected to the boundary conditions in equations (12) were solved numerically using Spectral collocation Method. The obtained results are displayed through graphs figures 2-35for dimensionlessvelocity, dimensionlesstemperature and dimensionless Nanoparticle concentration profiles were studied, as well as the skin friction coefficient, local Nusselt and Sherwood numbers.

Figs. 1-4 are plotted to examine the influence of slip parameter on both velocity profile and the magnitude of the Skin friction coefficient, it was observed that an increase in slip parameter reduced the velocity of the fluid flow and the magnitude of the Skin friction coefficient increased. Figs. 5-8 illustrate the effect of slip parameter on temperature and nanoparticle concentration profiles and it was shown graphically that an increase in slip parameter increased both temperature and nanoparticle concentration profiles. Figs. 9-12, it is easy to notice that temperature and nanoparticle concentration profiles decrease with an increase in thermal slip parameter. Figs. 13-16, indicate the effect of concentration slip parameter on temperature and

nanoparticle concentration profiles for $\beta = 0.5\ and\ \infty$, it was observed that there is a slit effect of concentration slip parameter on temperature profile while there is a significant effect on nanoparticle concentration profile. Figs. 17-20,show the enhancement of temperature and nanoparticle concentration and its associated boundary layer thickness with an increase in N_b. Figs. 21-24, represent the effect of Brownian motion parameter on temperature and nanoparticle concentration profiles; it was noticed in figs. 21-22 that increase in N_b leads to increase in temperature profiles for both $\beta = 0.5\ and\ \infty$, while a decrease in nanoparticle concentration profiles was observed with an increase in Nb for both $\beta = 0.5\ and\ \infty$. Figs. 25-28, depict the effect of chemical reaction on nanoparticle concentration profiles when $N_b = 0.1, 0.5$ and it can seem clear from the graphs that increase in chemical reaction depreciates the nanoparticle concentration. Figs. 29-32, display the behaviour of $N_t$on temperature and nanoparticle concentration profiles. It was indicated that an increase in N_t causes increases in both temperature and nanoparticle concentration when $Le = 1\ and\ 5$. Figs. 33-36, are sketched to analyse the influence of N_b on temperature and nanoparticle concentration, and for $Le = 1$, both temperature and nanoparticle concentration decrease as Nb increases, while the increase in $N_b\ for\ Le = 0.5$ enhanced the temperature profile and the reverse was noticed in nanoparticle concentration. It was discovered from figure 37 that the temperature profile is enhanced with an increase in Eckert number. Since the increase in Eckert number leads to an increase in thermal energy which improves the temperature and thermal boundary layer thickness nanofluid.

Figs. 38, it is observed that the rise in Eckert number near the surface cause a decrease in the concentration distribution, while the reverse is indicated away from the surface for$\beta = 0.5$. Figs. 39-40, portray the behaviour of Hartman number H_a on both temperature and nanoparticle concentration for $\beta = 0.5\ and\ \infty$, and it observed that there is an increase in both profiles when there is an increase in Ha. Figs. 41-42 represent the effect of Brownian motion Nb and Hartman number$H_a$on local Nusselt number ($-\theta(0)$) and $-\phi'(0)$, while an increase in N_b causes decreases in local Nusselt number and increase in Nb leads to an increase in $-\phi'(0)$. Figs. 43-44, are plotted to see the behaviour of Brownian motion and Eckert number on both $-\theta(0)$ and$-\phi'(0)$, and it shows graphically that there is a decrease in local Nusselt number and increases in Sherwood number as we increase the value of the Brownian motion parameter.

Table 1: Numerical values of $\left(1 + \frac{1}{\beta}\right) f''(0),\ -\theta', and\ -\phi'(0)\ with\ \lambda, \gamma, \delta, \beta\ for\ N_t = N_b = 0.1, E_c = X = 0.2, Le = 5, and\ P_r = 3$

λ	γ	δ	β	$\left(1 + \frac{1}{\beta}\right) f''(0)$	$-\theta'(0)$	$-\phi'(0)$
0	0.1	0.1	0.5	-1.743300	0.652945	1.37517
1	0.1	0.1	0.5	-0.537442	0.490495	1.05486
3	0.1	0.1	0.5	-0.242811	0.375805	0.9233303
0.1	**0**	0.1	0.5	-1.37247	0.6473183	1.28569
0.1	**0.8**	0.1	0.5	-1.37247	0.425237	1.34874
0.1	**40.1**	0.5		-1.37247	0.168251	1.41875
0.1	0.1	**0**	0.5	-1.37247	0.756331	1.21216
0.1	0.1	**0.5**	0.5	-1.37247	0.281242	1.50214
0.1	0.1	**3**	0.5	-1.37247	-0.0122779	1.53373
0.1	0.1	0.1	**0.3**	-1.367733	0.631137	1.29903
0.1	0.1	0.1	**4**	-0.759598	0.602165	1.27278
0.1	0.1	0.1	∞	-0.914972	0.478581	1.27365

Table 2: Numerical values of $-\theta'(0)$ and $-\phi'(0)$ with N_t, N_b, X, and E_c for $\lambda = \gamma = \delta = 1\ \beta = 0.5, P_r = 3, and\ Le = 5$

N_t	N_b	X	E_c	$-\theta'(0)$	$-\phi'(0)$
0.1	0.1	0.1	0.1	0.698104	1.27562
0.5	0.1	0.1	0.1	0.465085	1.28115
0.9	0.1	0.1	0.1	0.3150585	1.78684
0.1	**0.1**	0.1	0.1	0.698104	1.27562
0.1	**0.3**0.1	0.1	0.499445	1.43289	
0.1	**0.5**	0.1	0.1	0.344926	1.45705
0.1	0.1	**-0.3**	0.1	0.711315	0.564284
0.1	0.1	**0**	0.1	0.700414	1.13417
0.1	0.1	**0.5**	0.1	0.692182	1.71166
0.1	0.1	0.1	**0.1**	0.698104	1.27562
0.1	0.1	0.1	**0.3**	0.448205	1.41412
0.1	0.1	0.1	**0.6**	0.0638096	1.62865

5. CONCLUSIONS

In the present study, the heat and mass transfer in a Cassonnanofluid flow over a stretching sheet with the inclined magnetic field and slip boundary condition is investigated numerically. The concluding facts for the present study after a thorough observation are stated below.

1. Enhancement of both temperature and nanoparticle concentration was observed when there is an increase in thermophoresis parameter Nt.
2. Increase in slip parameter result to decrease in the velocity of the fluid
3. The chemical reaction for $X < 0$ increase the nanoparticle concentration and concentration boundary layer thickness but the reverse is observed for $X > 0$
4. Both temperature and nanoparticle concentration profiles increase with an increase in the magnetic field.

Conflict of interests

On behalf of all authors, the corresponding author states that there is no conflict of interest.

REFERENCES

[1] Choi, S. U. S., "Enhancing Thermal Conductivity of Fluids with Nanoparticle, In D.A. Signer, H.P.Wang Eds.," *Developments and Applications of Non-Newtonian Flows*, **231**, pp.99□105 (1995).

[2] Kandikar and Salman (2003). Convection heat transfer in microchannels using conventional fluids like water and ethylene glycol.Heat Transfer, Vol. 125, pp.151-155.

[3] Hu, C.; Bai, Ml.;Lv, J.; Li, X. (2014). Molecular dynamics investigation of the effect of copper nanoparticle on the solid contact between friction surfaces. Appl. Surf. Sd., 321, 302-309. [CrossRef]

[4] Mustafa, M. and Haynt. T. (2013)."UNSTEADY BOUNDARY LAYER FLOW OF NANOFLUID PAST AN IMPULSIVELY STRETCHING SHEET" Journal of Mechanics, Vol. 29, No, 3.

[5] Clement Kleinstreuer and ZelinXu, (2016). "Mathematical Modeling and Computer Simulations of Nanofluid Flow with Applications to Cooling and Lubrication" Fluids, 1, 16; doi:10.3390/fluidslO200l6.

[6] Alloui, Z., Vasseur, P. and Reggio, M. (2012). "Analytical and numerical study of buoyancy-driven convection in a vertical enclosure filled with nanofluid" Heat Mass Transfer 48:627-639.

[7] Y.M. Xuan, Q. Li, Investigation on convective heat transfer and flow features ofnanofluids, ASME J. Heat Transfer 125 (2003) 151–155.

[8] Bhattaryya, K. (2013). "MHD stagnation-point flow of Casson fluid and heat transfer over a stretching sheet with thermal radiation" Journal of Thermodynamics, Article ID169674.

[9] Khalid, S., Kamal, M.A., Rasheed, U. Farooq, S., Kussain, S. and Waqas, H. (2017). "Buoyancy and the Chemical Reaction Effects on MI-ID Flow of Casson Fluids through a Porous Medium Due to a Porous Shrinking Sheet" .1 Appl. Environ. Biol. Sci., 7(5)154-165.

[10] Mahanthesha, B. and Gireesh, B.J. (2018). "Thermal Marangoni convection in a two-phase flow of dusty Casson fluid" Results in Physics 8: 537—544.

[11] Naveed Ahmed,Umar Khan,Sheikh Irfanullah Khan, SaimaBano Syed TauseefMohyud-Din, (2017). "Effects ofthe magnetic field in squeezing flow of a Casson fluid between parallel plates" Journal of King Saud University — Science 29, 119-125.

[12] Sathies Kumar, P. and Gangadhar, K. (2015). "Effect of chemical reaction on slip flow of MHD Casson

fluid over a stretching sheet with heat and mass transfer" Advances in Applied Science Research, 6(8):205-223.

[13] Samir Kumar Nandy, (2013) "Analytical Solution of MHD Stagnation-Point Flow and Heat Transfer of Casson Fluid over a Stretching Sheet with Partial Slip, Hindawi Publishing Corporation, Article ID 108264, 9 pages.

[14] Waqar A. Khan, J. Richard Culham and 0. Daniel Makinde, (2015)j "Combined Heat and Mass Transfer of Third-Grade Nanofluids over a Convectively-Heated Stretching Permeable Surface" Can. J. Chem. Eng. 93:1880-1888.

[15] Hussain, T., Hayat, T. and Ramzan, M. (2016) "Flow of Cassonnanofluid with viscous dissipation and convective conditions: A mathematical model," J Cent. South Univ.,22: 1132-1140.

[16] Rizwan U Haq, SohailNadeem, ZafarHayat Khan, Toyin Gideon Okedayo, (2014). "Convective heat transfer and MUD effects on Cassonnanofluid flow over a shrinking sheet" Cent. Fur. 3. Phys. 1202), 862-871.

[17] Oyelakin, 1.S., Mondal S. and Sibanda, P. (2016). "Unsteady Cassonnanofluid flow over a stretching sheet with thermal radiation, convective and slip boundary conditions,"Alexandria Engineering Journal, 55, 1025-1035.

[18] Ghosh S-and Mukhopadhyay, S. (2017). "MI-ID slip flow and heat transfer of Cassonnanofluid over an exponentially stretching permeable sheet," International Journal of Automotive and Mechanical Engineering, Vol. 14, No. 4, pp. 4785-4804.

[19] Sidra Aman, SyazwaniMohdZokri, Zulkhibri Ismail, MoMZukiSalleh, Ilyas Khan, (2018). "Effect of MHD and Porosity on Exact Solutions and Flow of a Hybrid CassonNanofluid" Journal of Advanced Research in Fluid Mechanics and Thermal Sciences 44, Issue 1, 13 1-139.

[20]T. Javed and I. ''Mustafa, Slip effects on a mixed convection flow of a third-grade fluid near the orthogonal stagnation point on a vertical surface,'' *Journal of Applied Mechanics and Technical Physics, Vol. 57, No. 3, pp. 527–536, 2016.*

[21] T.Hayata,b, M. IjazKhana, SumairaQayyuma, A.Alsaedib, M. ImranKhanc. '' New thermodynamics of entropy generation minimization with nonlinear thermal radiation and nanomaterials'' Physics Letter A (in press), 2018.

Sciences & Technology **Vol 5 – N°1**, June 2020, pp. 29 -33

REMOVAL OF HEXAVALENT CHROMIUM BY EUCALYPTUS LEAF POWDER: OPTIMIZATION BY TAGUCHI METHOD

Submited on 29/01/2020 – Accepted on 05/05/2020

Abstract

Batch adsorption process of metal pollutants in aqueous phase can be influenced by several parameters such as initial pH of the solution, dose of the adsorbent, concentration of the adsorbate, contact time, temperature, agitation rate and adsorbent characteristics. In this study Taguchi's statistical approach was used to optimize the parameters of Cr(VI) biosorption by eucalyptus leaf powder. The orthogonal array L9 with three levels was applied to determine the optimal conditions for adsorption. The obtained results show that Cr(VI) removal is maximum (96.51%) with the low level of initial pH solution (1.0) and initial metal concentration (50 mg/L) and, with the high level of the adsorbent dose (3.0 g/L) and contact time (70 min). The analysis of variance of the experimental results, carried out for a level of significance of 5%, revealed that the initial pH solution is the most important parameter influencing the adsorption efficiency of chromium (VI) with a percentage contribution of 47.60%.

Keywords: Chromium (VI), eucalyptus leaf powder, adsorption, optimization, Taguchi method.

S. AZIRI *
N. BERKANE
H. BOUZETINE
S. MEZIANE

Laboratory of Applied Chemistry and Chemical Engineering, Faculty of Science, University Mouloud Mammeri of Tizi-Ouzou, Algeria.

* sabrina.aziri@gmail.com

INTRODUCTION

After its discovery in 1797–1798, chromium (Cr) and its salts found a wide range of applications in the chemical industry, graphics industry, tanning industry, artistic paints, anticorrosion paints, electroplating, steel alloys, stainless steel welding, and a multitude of other uses [1,2]. For the last 15 years, chromium has been classifed among the 20 most lethal environmental contaminants [3]. Epidemiological studies have shown that occupational and environmental exposure to metals such as chromium was associated with increased risk of various cancers and adverse health effects [4]. Chromium, which is strongly influenced by redox conditions, exists in the aquatic environment in an equilibrium between Cr(VI) and Cr(III). Cr(VI) is highly soluble, carcinogenic and 100 times more toxic than Cr(III) [5], which has been suggested to be essential for the maintenance of normal glucose tolerance in animals and humans.

Hexavalent chromium is an example of transport into the cells followed by metabolic reduction to trivalent chromium that is assumed to induce mutations and ultimately carcinogenesis by a direct reaction with deoxyribonucleic acid (DNA) [6,7].

Hexavalent chromium can also cause severe infections such as, skin and lung cancers, hepatic diseases and bronchial tract infections [8]. According to the recommendation of the World Health Organization [9], the maximum allowable limit for Cr(VI) in drinking water is at the level of 0.05 mg/L and its concentration in industrial wastewaters varies from 0.5 to 270 mg/L.

During the industrial processes, unused chromium salts are usually discharged in the final effluents, which causing a serious threat to the environment. Therefore, it is indispensable to remove Cr(VI) from wastewater before being released into the environment. In order to improve the removal efficiency of Cr(VI) from wastewater, numerous methods have been developed including chemical precipitation and electro-precipitation method, electrocoagulation, membrane filtration, ion exchange and electrochemical ion exchange process, liquid-liquid extraction, electrodialysis, phytoremediation in constructed wetland, infiltration percolation, photocatalysis and adsorption [10].This last is one of the attractive processes because of its high efficiency, flexibility, simplicity of design and operation without secondary toxic slurries [11]. Many investigations have been carried out on the effective removal of heavy metals from solution using natural adsorbents derived from agricultural wastes [12, 13, 14, 15].

However, optimization of parameters involved in this process plays a key role in maximizing the sorption efficiency. Statistical design of experimental methods provide an easier and equally efficient approach to optimize several operational variables [16]. The design of experimental (DOE) methods lead to more information after running fewer experiments. These methods included full factorial method, response surface method, Taguchi method and mixture method. The advantages of Taguchi method over the other methods are that numerous factors can be simultaneously optimized and more quantitative information can be extracted from fewer experimental trials [17]. This method which was widely used in improving the quality of manufactured goods and now being used in various other fields, and particularly for process parameters optimisation in wastewater treatment

studies contaminated by organiques [18, 19, 20] and inorganiques [16, 17, 21, 22] polluants.

The present study aims to investigate the possible use of eucalyptus leaves, an agricultural waste material, for the removal of hexavalent chromium ions from aqueous solution.Taguchi's statistical approach was applied to optimize the adsorption process.

2. MATERIAL AND METHODS

2.1. Adsorbent and Adsorbate

In this study, the eucalyptus leaves (EL) were used as a biosorbent for Cr(VI) removal from aqueous solution. The EL were dried in an oven at 80°C for 24h and grounded in a mortar. The obtained powder was first washed several times with hot water, and then rinsed with distilled water. After drying in an oven (Memmert, Germany) at 80°C until a constant weight was achieved, the eucalyptus leaf powder (ELP) was stored in hermetic bottle until use.

An aqueous stock solution (1000 mg/L) of Cr(VI) ions was prepared by dissolving potassium dichromate salt $K_2Cr_2O_7$ in distillated water. The stock solution of Cr(VI) was diluted with distilled water to obtain the required initial concentration Cr(VI) solutions.

2.2. Batch Adsorption Studies

Adsorption experiments were carried out by introducing a given quantity of ELP in a cylindrical reactor containing 50 mL of hexavalent chromium solution. The reactor was placed in a temperature-controlled water bath. The mixture was agitated using a mechanical stirrer at a constant stirring speed (250 rpm) and temperature (25°C) and filtrated using Whatman filter paper (N°3), after a fixed agitation time. The residual concentration of Cr (VI) was determined spectrophotometrically at 540 nm using a double beam UV–visible spectrophotometer (SHIMADZU UV-1601PC) after complexation with 1.5 diphenylcarbazide in an acidic medium [23].

The percentage of chromium removal, R (%), was determined as follows:

$$R(\%) = \frac{(C_0 - C_e)}{C_0} \times 100 \qquad (1)$$

Where C_0 and C_e represent the initial and final chromium (VI) concentrations (mg/L), respectively.

2.3 Taguchi method

The Taguchi method uses a statistical measure of performance called signal-to-noise (S/N) ratio.Usually, three types of S/N ratio analysis are applicable, namely: larger-the-better, nominal-the-best, and smaller-the-better types [24]. As the goal of this study was to remove Cr(VI) from wastewater by ELP, the larger-the-better quality characteristic was selected. The related S/N ratio is given by the following equation:

$$S/N = -10 \times \log\left(\frac{1}{r}\sum_{i=1}^{r}\frac{1}{R_i^2}\right) \qquad (2)$$

where r is the number of repetitions under the same experimental conditions, and R_i is the result of each repeated measurement, which is the Cr(VI) removal percentage.

In this study, each run was repeated three times. With the four three-level parameters, L9 orthogonal array design was chosen to perform the experiments. The four selected factors including initial pH of solution, initial concentration of Cr(VI), dose of adsorbent and time of contact. These parameters and their levels are given in Table 1.

***Table 1**.Parameters and their levels.*

Parameters	Symbols	Levels		
		1	2	3
Initial pH of solution	pH_0	1.0	2.0	3.0
Dose of adsorbent (g/L)	D	0.2	1.6	3.0
Initial concentration of Cr(VI)(mg/L)	C_0	50	100	150
Time of contact (min)	t	10	40	70

The analysis of variance is used to determine which factors have a significant effect at a given risk level on the quality characteristic. It also serves to determine the percentage contribution of each factor on the adsorption process [25].

3. RESULTS AND DISCUSSION

3.1. Global analysis of the obtained results

The experimental results of the adsorption yield of Cr (VI) on the powder of eucalyptus leaves and the calculated values of the (S/N) ratio are presented in Table 2. The results show a large variation in the average yield (R_m) of adsorption. Under the experimental conditions, average yield varied from 5.85 to 77.92% and the corresponding change in S/N ratio is 15.32 à 37.83.

***Table 2.** Experimental results and S/N ratio values for Cr(VI) removal*

Essay	Controllable factors in coded values				Removal(%)				S/N ratio
	pH_0	D	C_0	t	R_1	R_2	R_3	R_{moy}	
1	1	1	1	1	14.53	13.75	14.15	14.14	23.00
2	1	2	2	2	57.30	58.09	57.52	64.79	35.21
3	1	3	3	3	77.87	78.66	77.22	77.92	37.83
4	2	1	2	3	21.37	21.89	21.36	21.54	26.66
5	2	2	3	1	14.29	14.35	13.93	14.19	23.04
6	2	3	1	2	55.99	54.44	54.86	55.10	34.82
7	3	1	3	2	5.56	6.04	5.94	5.85	15.32
8	3	2	1	3	16.89	16.71	16.78	16.79	24.50
9	3	3	2	1	9.46	9.06	10.63	9.72	19.69

3.2. Effect of parameters on Cr(VI) removal

Table 3 shows the mean S/N ratio values for each level of the controllable parameters. As can be seen in this table and according to the higher mean (S/N) ratio base, the optimal conditions for Cr(VI) removal are initial pH solution at level 1 (1.0), adsorbent dose at level 3 (3.0 g/L), initial metal concentration at level 1 (50 mg/L) and contact time at level 3 (70 min). Thus, the optimal combination of process parameter levels for maximum removal of Cr(VI) is $pH_{01}D_3C_{01}\ t_3$. The representation of the main effects of each individual parameter at different levels is given by Figure 1.

Table 3. *Mean S/N ratios and main effects of design parameters*

Parameters	Mean (S/N) ratios			L3-L1
	L1	L2	L3	
pH_0	32.02	28.17	19.84	-12.18
D	21.66	27.58	30.78	9.12
C_0	27.44	27.19	25.40	- 2.04
t	21.91	28.45	29.67	7.76

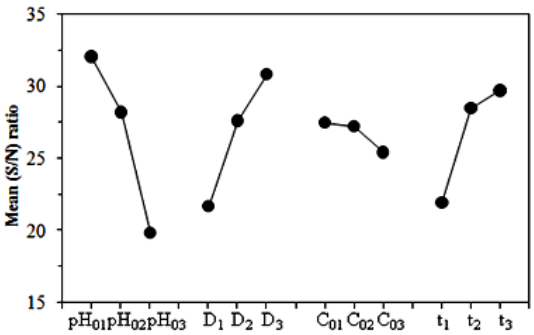

Figure 1*: Main effects of parameters which each parameter is at a given level*

3.3. Analysis of variance

Analysis of variance (ANOVA) is a statistical method that uses the Fischer test (F-ratio) to determine the impact of each parameter on the adsorption process and its contribution to the total variance of all design parameters [26].

The analysis of variance of the experimental results of the adsorption of chromium (VI) by EL powder is given in Table 4. This analysis was performed with a 95% confidence level. A parameter is considered significant on the response if the value of its F-ratio is higher than the critical value given by the Fisher table.
If the degree of freedom of the error is equal to zero, the calculation of F-ratio is not possible. To estimate the variance of the error, in this case, the sum of the squares of the error is replaced by the pooling of the sum (s) of the lowest square (s) of the parameter (s) [27]. This case is specific to orthogonal tables whose degree of freedom (df) is equal to the sum of the degrees of freedom of the design parameters.

According to the obtained results, the initial pH of the solution, with an F-ratio value of 31.19, well higher than the critical value (19.00) given by the Fisher table, is considered to be the most influential parameter on the adsorption efficiency of chromium (VI). This parameter is also the one with the highest percentage of contribution (ρ_F). This clearly indicates that the adsorption of chromium (VI) on the studied biosorbent is significantly influenced by the initial pH of the solution unlike the other selected parameters, as it determines the ionic species present in solution and the surface charge of the adsorbent [28,29]. These results are consistent with those of previous studies on the removal of heavy metals in the aqueous phase by different biosorbents [24, 30].

For the other parameters, i.e., the adsorbent dose and the contact time, they are significant for a 90% confidence level since the calculated values of F-ratio (17.23 and 14.01, respectively) were higher than the critical value given by the Fisher table (9.00). The ranking of the parameters in descending order of their percentage contribution on the adsorption process is pH_0>D>t. The contribution of each factor on Cr(VI) biosorption by the powder of eucalyptus leaves is given in Figure 2.

Table 4*. Analysis of variance for chromium(VI) removal using ELP.*

Factors	df	SS_F	V	F-ratio	SS_F'	ρ_F (%)
pH_0	2	232.510	116.25	31.19*	225.106	47.60
D	2	128.406	64.203	17.23**	120.952	25.58
C_0	2	7.454	3.727			
t	2	104.399	52.199	14.01**	96.945	20.51
Error	0					
Pooled error	2	7.454	3.727			6.31
Total	8	472.768				100

F(0.05,2,2) = 19.00 ; * Significant at 95% , F(0.1,2,2)= 9.00 ; ** Significant at 90%
SS_F: sum of squares of factors; V: variance; SS_F':sum of squares corrected

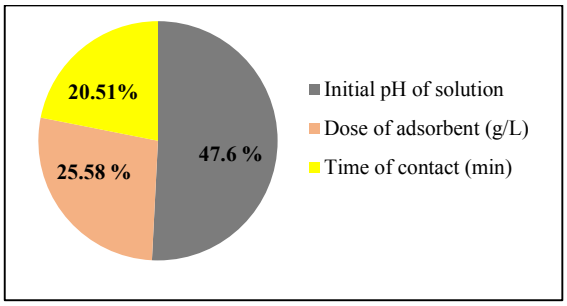

Figure 2*: Relative contribution of each factor (%) on Cr(VI) biosorption*

3.4. Confirmation experiments

The final step of Taguchi method is performing confirmation experiments to evaluate quality characteristics.The predicted $(S/N)_{opt}$ ratio using the optimal level of the process parameters, can be calculated as given:

$$(S/N)_{opt} = (S/N)_m + \sum_{i=1}^{k} \left(\left(\overline{S/N}\right)_i - (S/N)_m \right) \quad (3)$$

where $\overline{(S/N)}$ is the mean value of S/N ratio at the optimum level of the parameter, $(S/N)_m$ is the average value of the S/N ratios and k is the repetition of each optimum level of the parameter.

Five confirmation experiments were conducted using the optimal combination of process parameters. Predicted and experimental values of the S/N ratio and elimination efficiency are reported in Table 5. The results show that there is a good agreement between the values predicted by the model and the values determined experimentally.

Table 5.*Results of confirmation experiments for Cr(VI) removal*

	Optimal removal parameters	
	Predict	Experiment
Level	$pH_{01}D_3t_3$	$pH_{01}D_3C_{01}t_3$
% Removal	90.27	96.51
S/N Ratio	39.11	39.69

4. CONCLUSION

In this study, Taguchi L_9 (3^4) orthogonal array experimental design was applied to determine the optimum operating conditions for the adsorption of hexavalent chromium on eucalyptus leaf powder.

The results indicated that the Taguchi method gives a suitable approach for optimization of removal percentage of Cr (VI) under experimental conditions studied. The maximum percentage of Cr(VI) removal (96.51%) was at $pH_0 = 1$, initial Cr(VI) concentration = 50 mg/L, adsorbent dose of 3.0 g/L and time of contact = 70 min. The influence of the parameters in descending order is pH_0>D> t. The initial solution pH has the greatest contribution (47.60%) in the removal of Cr(VI) by ELP.

5. REFERENCES

[1] Pradhan D, Sukla L.B, Sawyer M, Rahman P.K, Recent bioreduction of hexavalent chromium in wastewater treatment: a review. J. Ind. Eng. Chem. 55:1, (2017)

[2] Niazi L, Lashanizadegan A, Sharififard H, Chestnut oak shells activated carbon: Preparation, characterization and application for Cr (VI) removal from dilute aqueous solutions. J. clean. Prod. 185:554, (2018)

[3] Bharagava R.N, Emerging Eco-friendly Green Technologies for Wastewater Treatment, (2020)

[4] Costa M, Klein C.B, Toxicity and carcinogenicity of chromium compounds in humans. *Critical reviews in toxicology 36*(2):155, (2006)

[5] Kumar V, Dwivedi S.K, Hexavalent chromium stress response, reduction capability and bioremediation potential of Trichoderma sp. isolated from electroplating wastewater. Ecotox. Environ. Safe. 185, (2019) 109734

[6] Gunnar F.N., Bruce A.F, Monica N, Lars F, Handbook on the Toxicology of Metals. 3rd Edition, Academic Press (2007)

[7] Saha R, Nandi R, Saha B, Sources and toxicity of hexavalent chromium. J. Coord. Chem. 64(10):1782, (2011)

[8] Ali A, Saeed K, Mabood F, Removal of chromium (VI) from aqueous medium using chemically modified banana peels as efficient low-cost adsorbent. Alexandria Eng. J. 55(3):2933, (2016)

[9] WHO Guidelines for drinking-water quality. 3rd ed. Switzerland: World Health Organization Geneva (2008)

[10] Oumani A, Mandi L, Berrekhis F, Ouazzani N, Removal of Cr^{3+} from tanning effluents by adsorption onto phosphate mine waste: Key parameters and mechanisms. J. hazard. Mater. 378, 120718, (2019)

[11] Xia S, Song Z, Jeyakumar P, Bolan N, Wang H, Characteristics and applications of biochar for remediating Cr(VI) contaminated soils and wastewater. Environ. Geochem. Hlth. 1,(2019)

[12] Nasseh N, Taghavi L, Barikbin B, Harifi-Mood A.R, The removal of Cr (VI) from aqueous solution by almond green hull waste material: kinetic and equilibrium studies. J. Water Reuse Desal. 7(4): 449, (2016)

[13] Sharma S.K, Mahiya S, Lofrano G, Removal of divalent nickel from aqueous solutions using Carissa carandas and Syzygium aromaticum: isothermal studies and kinetic modelling. Appl. Water Sci. 7(4):1855, (2017)

[14] Heraldy E, Lestari W.W, Permatasari D, Arimurti D.D, Biosorbent from tomato waste and apple juice residue for lead removal. J. environ. Chem. Eng. 6(1): 1201, (2018)

[15] Shakya A, Agarwal T, Removal of Cr (VI) from water using pineapple peel derived biochars: Adsorption potential and re-usability assessment. J. Mol. Liq. 293, 111497, (2019)

[16] Pundir R, Chary G.H.V.C, Dastidar M.G, Application of Taguchi method for optimizing the process parameters for the removal of copper and nickel by growing Aspergillus sp. Water resour. Ind. 20:83, (2018)

[17] Floutya R, El-Khourya J, Maatouka E, El-Samrania A, Optimization of Cu and Pb biosorption by Aphanizomenon ovalisporum using Taguchi approach: kinetics and equilibrium modeling. Desal. Water Treat. 155:259, (2019)

[18] Chen Z, Deng H, Chen C, Yang Y, Xu H, Biosorption of malachite green from aqueous solutions by Pleurotus ostreatus using Taguchi method. J. Environ. Hlth. Sci. Eng. 12(1), 63, (2014)

[19] Berkane N, Meziane S, Aziri S, Optimization of Congo red removal from aqueous solution using Taguchi experimental design. Sep. Sci. Tech. 55(2):278, (2020)

[20] Gholami-Bonabi L, Ziaefar N, Sheikhloie H, Removal of phenol from aqueous solutions by magnetic oxide graphene nanoparticles modified with ionic liquids using

the Taguchi optimization approach. Water Sci. Tech. 81(2):228, (2020)

[21] Aziri S, Meziane S, Optimization of process parameters for Cr (VI) removal by seed powder of prickly pear (Opuntia ficus-indica L.) fruits using Taguchi method. Desal. Water Treat. 81:118, (2017)

[22] Daoud N, Selatnia A, Taguchi Optimization Method for Nickel Removal from Aqueous Solutions Using Non-living Pleurotus mutilus. Arab. J. Sci. Eng. 44(12):10067, (2019)

[23] Clesceri L.S, Greenberg A.E., Eaton A.D, Standard methods for the examination of water and wastewater, American Public Health Association. Washington DC 4-415, (1998)

[24] Yen H.Y, Li J.Y, Process optimization for Ni (II) removal from wastewater by calcined oyster shell powders using Taguchi method. J. Environ. Manage. 161: 344, (2015)

[25] Roy R.K.A, primer on the Taguchi method. New York: Von Nostrand Reinhold (1990)

[26] Yang W.P, Tarng Y.S, Design optimization of cutting parameters for turning operations based on the Taguchi method. J. mater. Process. Tech. 84(13):122, (1998)

[27] Phadke M.S, Quality engineering using design of experiments. In Quality control, robust design, and the Taguchi method. Springer, Boston, MA 31, (1989)

[28] Srividya K, Mohanty K, Biosorption of hexavalent chromium from aqueous solutions by Catla catla scales: equilibrium and kinetics studies. Chem. Eng. J. 155(3):666, (2009)

[29] Mahajan G, Sud D, Modified agricultural waste biomass with enhanced responsive properties for metal-ion remediation: a green approach. Appl. water sci. 2(4):299, (2012)

[30] Ramavandi B, Asgari G, Faradmal J, Sahebi S, Roshani B, Abatement of Cr (VI) from wastewater using a new adsorbent, cantaloupe peel: taguchi L_{16} orthogonal array optimization. Korean J. Chem. Eng. 31(12): 2207, (2014)

Sciences & Technology **Vol 5 – N°1**, June 2020, pp. 35 -39

THERMAL, PHYSICAL AND MECHANICAL PROPERTIES OF COMPOSITE POLYOXYMETHYLENE / CALCIUM CARBONATE (POM/CaCSQO$_3$)

Submited on 29/01/2020 – Accepted on 24/05/2020

Abstract

Polymers may replace advantageously the traditional materials of structure. We can distinguish among others their lightness, their moderate cost, their various processes which allow to implement and to shape them simultaneously. In the thermoplastic polymers case numerous are their peculiarities which make them interesting. The majority of studies of the thermoplastics and their composites become only attached to their mechanical properties; their behavior is more complex and establishes an obstacle major which requires more thorough studies. Our objective is the incorporation of a mineral filler the $CaCO_3$ in the polyoxyméthylene (POM) in the context of the development of a new composite material and to define its thermals, physical and mechanicals properties.

So,our work consists in studying the thermals, physical and mechanicals properties of the composite Polyoxymethylene / $CaCO_3$.

Keywords: thermal, physical and mechanicals, properties, Polyoxymethylene, CaCO3.

L. LATRECHE *
N. HADDAOUI

Laboratory of Physical Chemistry of High Polymers (LPC HP), University Ferhat Abbas Setif 1, Algeria.

* karilatrech@gmail.com

INTRODUCTION

The polyoxymethylene is a polymer also called POM according to the standard ISO. It exists either under copolymer (CPOM), or homopolymer (HPOM) shape, both forms differ little. The POM is an opaque semicristalline polymer and its natural color is white but it is often colored. The homopolymer shape presents slightly better mechanicals characteristics. It is marketed in various granules; the average thickness of a granule is about 3 mm [1, 2].The polyoxymethylene is one of the most important and widely used thermoplastics, filled with rigid inorganic fillers such as calcium carbonate to create high stiffness and modulus and/or to reduce the cost. Moreover, the development of POM and its composites or blends will improve thermal, physical and mechanical properties and allow a high percentage of use in different sectors [3-5].

$CaCO_3$ is one of the important fillers used in the industries of plastics, rubber and paint. One of the most problematic issues for the use of $CaCO_3$ is its hydrophilic property. Calcium carbonates are white, not toxic, insoluble powders in the pure water, but dissolve in the water charged of CO_2 gas. Calcium carbonates represent the most used filler on the plastic sectors [6]. A surface treatment of the calcium carbonate is essentially made to reduce the superficial tension and improve the dispersal of filler in the matrix. The modification of the surface by surfactants has been extensively studied. For example, the surfactants containing reactive functional groups such as silane coupling agents ,titanate coupling agents or stearic acid [7-10]can all improve the hydrophobic properties of $CaCO_3$.

2. EXPERIMENTAL PROCEDURE:

2.1. Materials:

-Polymer: The polymer used in this study was polyoxymethylene, it was supplied by Dupont de Nemours under the name Delrin HPOM it is a commercial granular homopolyoxymethylene , It has a density of 1.42 g/cm^3 and a melting flow index (MFI) of 1.70g/10 min, its melt temperature is about 165°C.

- Fillers: We used three different fillers: Calcium carbonate (CaCO3) used were provided by the Tunisian Society of Industrial Calcium Carbonate (STICC). Having been used in two different sizes, the corresponding trade names are HERMACARB 2FT and HERMACARB 5FN. The calcium carbonate (CaCO3) provided by STICC sold under the designation Hermacarb 2FT is a treated filler micronized with high purity and whiteness, while the calcium carbonate (CaCO3) sold under the name Hermacarb 5FN is untreated filler and characterized by its whiteness and purity, we treat the 5FN with stearic acid[5] and we called it (5FT) (Table 1).

Table 1: The chemical composition of $CaCO_3$, chemical analysis by X-ray diffraction revealed the following capacities for both types:

Name	*Symbols*	Weight composition (%)
Calcium carbonate	$CaCO_3$	99,92
Magnesium oxide	MgO	0,04
Titanium Dioxide	TiO_2	0,02
Potacium oxide	K_2O	0,01
Iron oxide	Fe_2O_3	0,01

Both varieties of calcium carbonate used mainly differ by their size. The physical properties of each type are as follows:

Table 2: The physical properties of the fillers:

Parameter	values for 2FT	values for 5FN
Moisture %	0,10	≤0,20
Density: g/cm^3	2,60	2,70
Average diameter of particle microns	2	5

2.2. Preparation of composite POM/$CaCO_3$:

$CaCO_3$ was dried in an oven at 100°C for 24 hours to ensure removal of moisture before using and premixed with POM, then specimens were prepared by melt mixing in a brabender plasticorder at a rotor speed of 60 rpm, at the temperature of 190°C.After that the composite was granulated into pellet by using granulator, then pellets were put into the mould and pressed at 25 bars during 8 minutes at moulding temperature of 190°C. Weight compositions used of POM / $CaCO_3$ were :(97.5/2.5, 95/5, 90/10, 85/15, 80/20, 75/25, 70/30).

3. CHARACTERIZATIONS:

3. 1. Thermal Characterization:

3.1.1. Heat distortion temperature (HDT):

The HDT was obtained in accordance with ASTM D648, which describes HDT as the temperature where a specimen (3 x 13 x 127 mm^3) deflects by 0.25 mm under 1.8 MPa while heated in an oil bath at a rate of 2 °C/min. At least 5 specimens were tested and the average value was used for the data plot.

3.1.2. Vicat softening temperature:

Vicat softening temperature tests (VST) were used to determine the softening temperature of the material. A Zwick Vicat softening temperature tester at 50 N force and 5 °C/min heating rate was used to determine temperature at which the indentor penetrates 1 mm into the material. At least 5 specimens were tested and the average value was used for the data plot.

3.2. Physical Characterization: Density measurement:

Density is measured with a pycnometer by weighing a substance, usually in the liquid state, that is placed in the device and fills the pycnometer to a mark on its neck or to the upper edge of a capillary tube, corresponding to the nominal volume of the pycnometer. The major advantages of the pycnometric method for the determination of density are high accuracy of measurement (to 10^{-5} g/cm^3).

3.3. Mechanical Characterization:

3.3.1. Hardness «Shore D»:

The test procedure followed ISO / 869, on a typical durometre D which is intended for the hard polymers. The test consists in applying to samples of (50/ 50/ 3 mm^3) in dimensions a penetrator of 5 kg and then we read directly the sinking after 10 seconds. The measures are made in the room temperature; the results are given by the average of five values so obtained.

3.3.2. Tensile test:

The tensile properties were determined using dumbbell specimens of (115×12.7 ×3 mm3) in dimensions. The test was carried out using a universal testing machine with a crosshead speed of 10 mm/min. The test procedure followed ASTM D 638-72. From the experimental stress–strain curves, tensile properties (modulus of elasticity and elongation at break) of the composite were calculated at room temperature. Five specimens were tested and the average values were used for the data plot.

3.3.3. Notched Izod impact strength:

Izod impact strength properties were determined at room temperature with a CEAST 6546/000 machine provided with a 15 J pendulum according to the ASTM D 256-73, and using specimens of (63×12.7×3 mm3) in dimensions . Specimens were molded with a notch radius of 0.5 mm. The radius was chosen such that the tip of the notch was located in the residual compressive zone. At least five specimens were tested and the average value was used for the data plot.

4. RESULTS AND DISCUSSION:

4.1. Thermal properties:

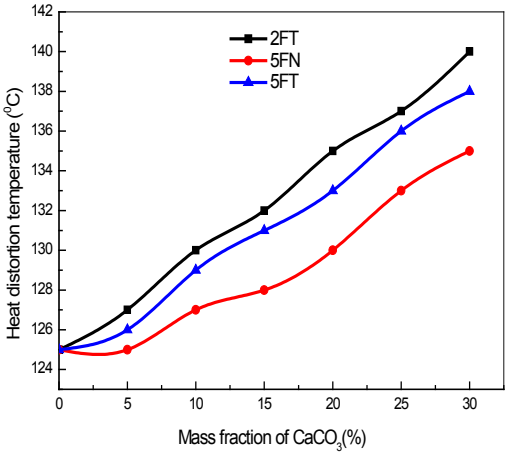

Figure 1: Heat distortion temperature of POM / $CaCO_3$ as a function of mass fraction of $CaCO_3$

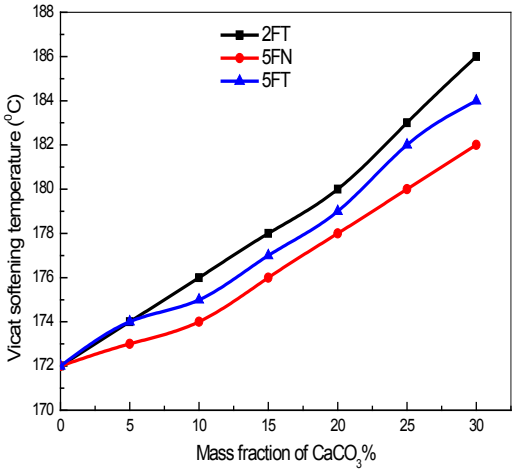

Figure 2: Vicat softening temperature of POM / $CaCO_3$ as a function of mass fraction of $CaCO_3$

The presence of filler changes the properties of the polyoxymethylene in the composite, it affects the molecular mobility and causes a certain order, the heat distortion temperature of POM/CaCO3 (HDT) can be offset, reduces the ability of macromolecular chains to move against each other causing an increase in the vicat softening temperature .Thermal tests can give very different results, depending on the exchange rate of CaCO3.Figures 1 and 2 show the variations of heat distortion temperature and the vicat softening temperature of the composite POM/CaCO3 when we vary the rate of CaCO3 ,thus varying the molecular mobility of polyoxymethylene in the composite. We noted that the heat distortion temperature, the vicat softening temperature gradually grow with the increase in the rate of CaCO3 that may be due to the increase of the order so the crystallinity within the material, these figures also show that the temperature of heat distortion temperature (HDT) and the vicat softening temperature of the composite POM/CaCO3 are influenced by the size and the treatment of fillers.

4.2. Density measurement:

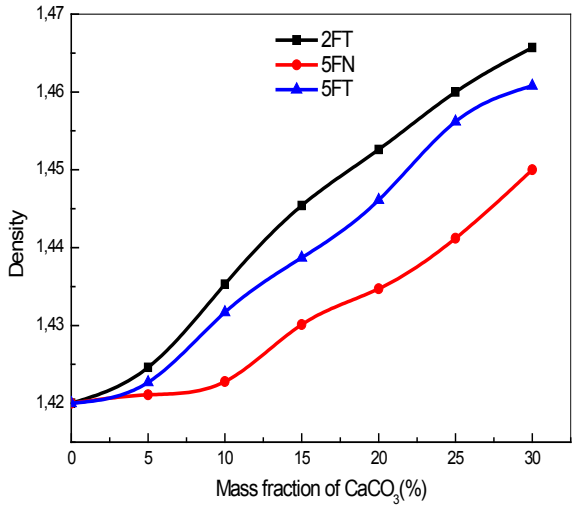

Figure 3: Density of POM / $CaCO_3$ as a function of mass fraction of $CaCO_3$

The Figure 3 shows the variations in the density of the composite POM/CaCO3 when we vary the rate CaCO3.Siegmann et al [11] without calculating the change in free volume, have speculated that the increase of heat distortion temperature (HDT) load being related to the decrease of the free volume. As the heat distortion temperature (HDT) and the density varied in the same way, the evolution of the (HDT) can be also partly due to the evolution of free volume with different heat treatments.

4.3. Mechanical properties:

4.3.1. Hardness «Shore D»:

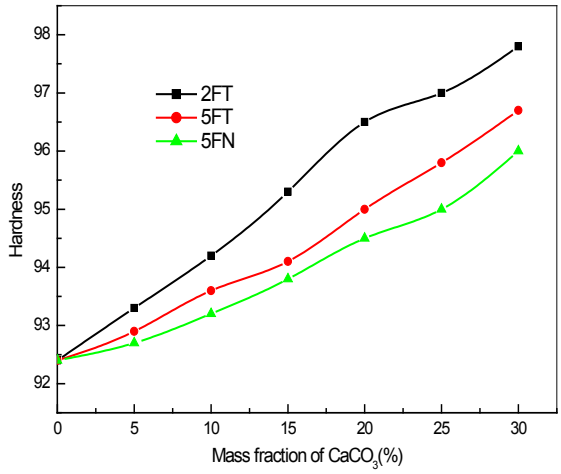

Figure 4: Hardness «Shore D» of POM / $CaCO_3$ as a function of mass fraction of $CaCO_3$

Changes in the Shore D hardness of the composite POM/ $CaCO_3$ with the rate of $CaCO_3$ are presented in the Figure

4. As observed, the hardness increases with increasing rate of $CaCO_3$. For low rate of $CaCO_3$, the macromolecules are least reorganized, it induces an increase of the free volume which lowers the hardness and therefore low density (ρ).According Van Krevelen [12] the density (ρ) is connected to the elasticity modulus (E): $E \propto \rho^7$. This means that the samples have a lower density also have a lower modulus of elasticity, as can be seen on the figure 5.Structural changes were also demonstrated by measuring their mechanical properties, from figures 5 and 6, we can see that the values of the modulus of elasticity of composites increase with the increase in the rate of $CaCO_3$. The effect of particle size and filler treatment is also well marked. Shore D hardness and modulus of elasticity vary in the same direction and depend on particle size and filler treatment. Composites POM/ $CaCO_3$ (2FT and 5FT) with treated fillers present better thermals, physical and mechanicals characteristics than composites with untreated fillers (5FN). Shore D hardness, density, modulus of elasticity of various composites POM/ $CaCO_3$ increase with increasing of $CaCO_3$ rate.

4.3.2. Tensile test:

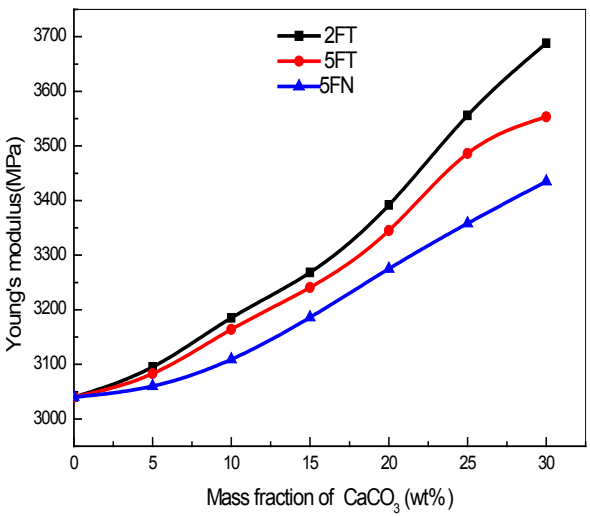

Figure 5: Modulus of elasticity of POM / $CaCO_3$ as a function of mass fraction of $CaCO_3$

Figure 5 shows that the young's modulus increases with the amount of CaCO3 introduced into the polyoxymethylene matrix. This curve means that the known particle size of CaCO3 and incompatibility between polyoxymethylene and CaCO3 problems do not come into play until a mass fraction of 5 % of CaCO3, modules change relatively little, it seems that the small amount of CaCO3 doesn't affect the mechanicals characteristics of the polyoxymethylene matrix, so the POM which is clear and especially in majority imposes its properties [13, 14]. From the mass fraction around 6% of CaCO3, the filler gradually gaining its strength characteristics and the young's modulus increase gradually. Figure 6 puts in evidence the variations of elongation at break of our composite with the rate of CaCO3 introduced and above shows the influence of the particle size (2FT and 5FT) and the treatment of fillers(5FN and 5FT).

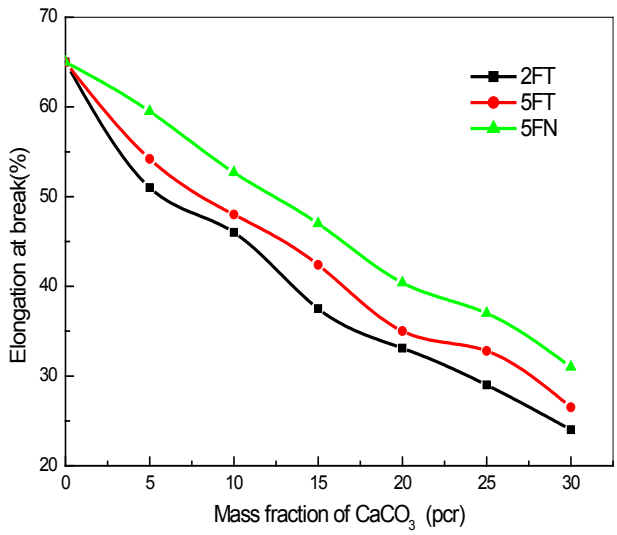

Figure 6: Elongation at break of POM / $CaCO_3$ as a function of mass fraction of $CaCO_3$

4.3.3. Notched Izod impact strength:

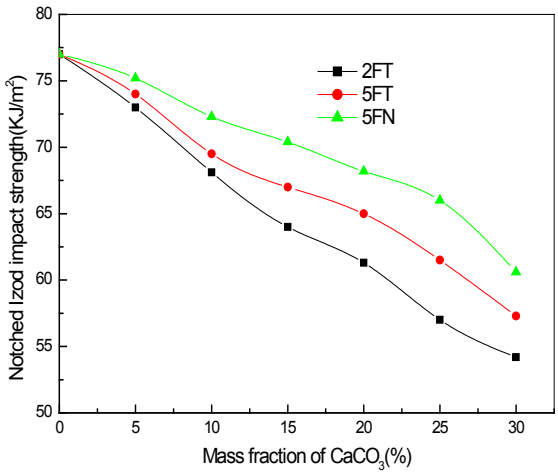

Figure 7: Notched Izod impact strength of POM / $CaCO_3$ as a function of mass fraction of $CaCO_3$

Figure 7 shows the evolution of the notched Izod impact strength of the composite POM/ $CaCO_3$ with the rate of $CaCO_3$, this notched Izod impact strength decrease with the increase of $CaCO_3$.The influence of filler treatment (5FN and 5FT) and the particles size(2FT and 5FT) appear on all properties studied. The notched Izod impact strength of composite POM/ $CaCO_3$ for low rates of $CaCO_3$increases which can be explained by an increased amount of amorphous therefore an increase in molecular mobility of this phase stage and therefore a reduction in

stiffness[14,15] . With high rates, it is observed that notched Izod impact strength of the composites decrease which can be attributed to the reduction of the molecular mobility of the amorphous phase reduced.

5. CONCLUSIONS:

The heat distortion temperature (HDT) and the vicat softening temperature gradually grow with the increase in the rate of $CaCO_3$ that may be due to the increase of the order so the crystallinity within the material.

A significant increase in the heat distortion temperature (HDT), the vicat softening temperature, density, Shore D hardness and young's modulus of the composite POM/$CaCO_3$ with increasing level of incorporation of the filler $CaCO_3$.

A relative decrease in elongation at break, notched Izod impact strength, this decrease which can be explained by an increased amount of amorphous therefore an increase in molecular mobility of this phase stage and therefore a decrease in rigidity.

The influence of treatment of the filler and the size of the particles appear on all properties studied.

6. REFERENCES:

[1] F. Pardos.Polyacetals (POM). In : Plastiques. Paris : Techniques de l'ingénieur, AM 3385, 2002

[2] W.Xu, P. P. He. Journal of Applied Polymer Science, 2001, 80,304

[3] Z.Tinxu, X.Agen. European Polymer Journal, 1999, 35, 1901

[4] Xiaodong .Wang, Xiuguo .Cui, European Polymer Journal 41(2005) 871–880

[5]L.Latreche, N.Haddaoui, M.E.Cagiao,Revue Roumaine de Chimie 62,3(2017)267-276.

[6] C.A. Naudin,C.Clozza,Charges. In : Plastiques et Composites. Paris : Techniques de l'ingénieur, A 3220, 2004

[7] Z. Demjén, B. Pukánszky, Journal of Colloid and Interface Science. 190(1997) 427–436.

[8]T. Nakatsuka, H. Kawasaki, K. Itadani, Journal of Applied Polymer Science. 27 (1982) 259–269.

[9]T.Nakatsuka, H.Kawasaki, K.Itadani, Journal of Colloid and Interface Science. 82 (1981) 298–306.

[10]L.Latreche ,N. Haddaoui, M. E.Cagiao ,Russian .Journal of Applied Chemistry 89,10(2016)1713-1721.

[11]A. Siegmann,A. Bouchman.and S.Kenig, Polymer Engineering and Science, 22, (1982) 40-47 [12] DW .Van Krevelen. Properties of Polymers: Amesterdam, Elsevier (1972).

[13]M.Arroyo,M.Ramos,M.Sanchez-Berna et J.P. Vigo Matheu, Journal of Polymer Engineering.9(1990)85-104

[14] V.Sabin-Chiarilli, J.Pabiot ,European Polymer Journal 36(2000) 1387–1399

[15]C. Albano, Journal of Composite Structures.48 (2000) 49-58.

Sciences & Technology Vol 5 – N°1, June 2020, pp. 41 - 44

THE USE OF LOCAL AND RENEWABLE PRODUCT IN THERMAL INSULATION.

Submited on 21/02/2019 – Accepted on 05/11/2019

Abstract

This work aims to develop a new eco-composite construction that is good thermal insulation with a simple and inexpensive method. The prepared material is Portland cement and date palm fibers. This was characterized by: Raman spectroscopy to study the impact of fibers on the chemical behavior of the matrix, the hot wire method for measuring thermal conductivity and Scanning Electron Microscopy (SEM) for porosity measurement. The comparison of the results with those of Portland cement reveals that the inclusion of date palm fibers has no impact on the chemical behavior of the matrix and that the addition of these fibers increases the porosity and decreases the thermal conductivity cement.

Keywords: *DPF, RAMAN, SEM thermal conductivity.*

BELLEL NADJOUA *
BOUFENDI TOUFIK

Energy Physics Laboratory, Université Frères Mentouri Constantine, Constantine, Algeria.

* bellel.nadjoua@gmail.com

INTRODUCTION

The overconsumption of energy in the heating and cooling of buildings has led researchers to think of sustainable construction. In the context of sustainable construction, the new regulations on thermal insulation in the field of construction encourage the development of new materials based on plant fibers to build energy-efficient buildings while ensuring the comfort of habitat [1].

Although Algeria is among the countries that have a multitude of plant materials (the date palm, cork, ...), the recovery of these materials remains insufficient mainly in the building sector [2].

In this study, we will discover the insulating power of the date palm (Figure.1) to enhance the local product while saving energy.

In Algeria, the number of date palm is more than 10 million trees [3]. This material contains several renewable parts, the estimated global production being greater than 1 200 000 tonnes of petioles, 410 000 leaves and 300 000 clusters per year [4]. Several studies have been done with natural materials and have shown that they are comparable to standard building materials [5].

Figure 1. image of a date palm

Kriker *et al* [6] developed a new material containing concrete and date palm fiber to evaluate the mechanical properties of this material. Benmansour *et al* [7] found that the use of DPF in the mortar provides a composite with good thermal resistance and mechanical properties that can be used in building construction as new insulating materials. Chikhi *et al* [8] found that gypsum reinforcement with 5% Date Palm Fiber (DPF) gives a composite with good thermal and mechanical properties making it a good candidate for the development of effective insulation materials safe. Recently, Chennouf *et al* [9] Confirmed that the introduction of (DPF) in reinforced concrete gives excellent hygrothermal properties.

In this work the characterization of the developed material will be done with the following methods: Raman spectroscopy to determine the chemical composition of the DPF and the new prepared material, the hot wire method to measure the thermo physical properties and the Scanning Electron Microscopy (SEM) to study the porosity of the material.
The results obtained showed the insulating power of cement based on date palm fiber.

II. EXPERIMENTAL

A. Materials:

A.1. Portland cement (PC) :

Portland cement **(CIMENT PORTLAND A LA POUZZOLANE CEM II/A-P 42,5 N)** is mainly composed of four different mineral phases: Tricalcium silicate (Alite) C_3S, Dicalcium silicate (Belite) C_2S, Tricalcium aluminate (Celite) C_3A and Tetracalcium alumino ferrite (Ferrite) C_4AF. This matrix was provided by the cement company "SCHB" of Hamma Bouziane-Constantine, a subsidiary of the industrial group of Ciments d'Algerie **"Groupe GICA"**.

A.2. Date palm fiber (DPF):

The renewable part of the date palm used in this study is the cluster that was collected at Biskra (Algeria), the choice of this part of the date palm was made for its thermophysical properties from the literature [2]. The cluster was dried at 60 ° C in the laboratory's Memmert oven for 24 hours and milled with an electric grinder until the fiber was obtained.

B. Sample preparation:

The prepared composite (BM5) is obtained by mixing Portland cement with a 5% concentration of date palm fiber. the prepared powder is analyzed with the methods: RAMAN and SEM and compared with pure portland cement (PC).

To measure the thermal conductivity of these samples with the hot wire method, two samples (BM5 and PC) of the same mass composed of Portland cement mixed with two mass fractions (0 and 5%) of DPF with progressive water addition corresponding to the weight of the added fibers. The mixtures are poured into molds of (10 cm × 10 cm × 10 cm). The samples were extracted from the molds after 72 hours and allowed to cure for 28 days in the laboratory under ambient conditions.

II. Characterization techniques

Horiba Raman spectrometer was used to characterize the molecular composition and external structure of the samples.

To measure the thermo-physical properties (conductivity, diffusivity and volume heat capacity) of the samples (CP and BM5) the transient hot wire method was used. The measurements are based on the analysis of the temperature response of the material analyzed at the heat flux pulses. The heat flow is excited by the electrical heating of the resistance inserted in the probe, which is in direct thermal contact with the test sample. The evaluation of thermal conductivity and volume heat capacity is based on periodically sampled temperature records, if the propagation of heat occurs in an unlimited medium [10].

Using Scanning Electron Microscopy (SEM), we observed pore geometry in order to study the impact of the addition of DPF fibers on the porosity of the matrix. The SEM analysis was conducted NeoScope JCM-5000.

III. RESULTS AND DISCUSSION :

A. RAMAN analysis :

The development of new bio-based materials requires prior knowledge of the chemical composition of the fibers used, which is why the Raman spectroscopy of DPF was done.

Figure 2 shows the Raman spectrum of DPF. The bands at 1115 and 814 cm^{-1} were respectively due to cellulose and pectin [11, 12, 13]. The lignin contribution was present at 1660 cm^{-1} [11, 12].

The Raman results of the two samples (PC and BM5) are shown in Figure 3. The phases of the samples were identified by the literature [14]. It can be seen in Figure 1 that the peaks in the two Ramanshift samples of 836, 885 and 1088 cm^{-1} correspond respectively to C_3S, C_2S and gypsum. Peak C_3A can be easily identified in both samples with a Raman shift of 551 cm^{-1}.

In the BM5 sample we notice a development of a broad characteristic peak of the cellulose which extends from 1110 cm-1 to 1190 cm-1. This explains that the DPF are well incorporated into the matrix.

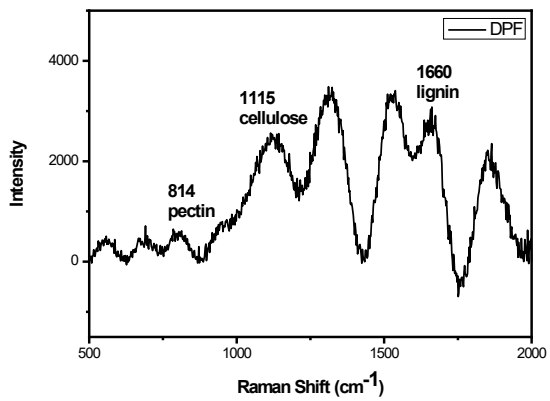

Figure 3. The Raman spectra of DPF.

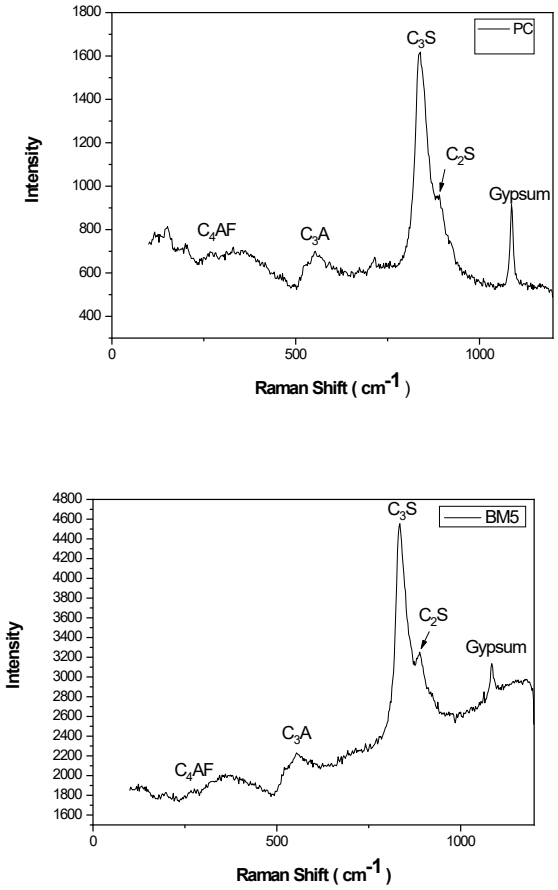

Figure 3. The Raman spectra of samples PC and BM5.

B. Thermal characterization:

Ten successive measurements were made for each sample to avoid measurement errors. The measurement results are presented in Table 1:

Table1. Thermal conductivity of samples

Samples	Thermal Conductivity (W/m.K)
PC	0,90
BM5	0,24

Table 1 shows the values of the thermal conductivity of the matrix before and after the addition of 5% of fibers. We note that the addition of DPF in the cement matrix considerably reduces the thermal conductivity of the composite. According to the results found, the decrease in thermal conductivity after the addition of 5% of fibers in Portland cement is 73.4%. This decrease was expected and is directly linked to the insulating nature of date palm fibers. Similar behavior was reported by Abani *et al* [15], they studied the impact of adding date palm fibers to the plaster. According to their results for a mass percentage of fiber of 5%, the reduction in thermal conductivity is approximately 36.67%.

From the results obtained in this work it can be concluded that the addition of date palm fibers in a cement matrix could considerably improve the thermal properties of the composites.

C. SEM analysis:

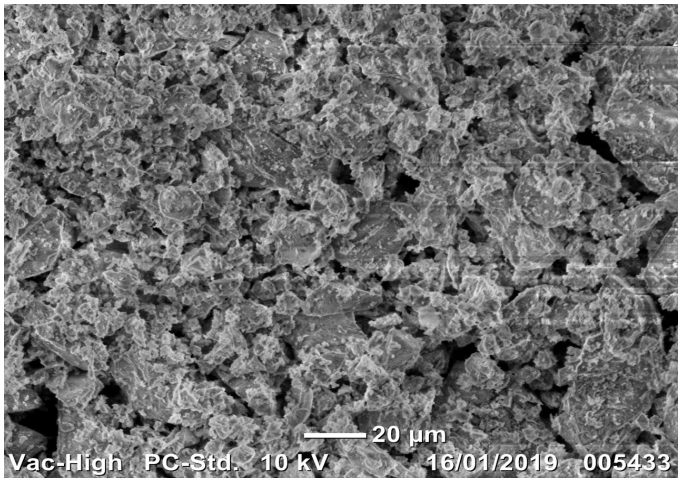

Figure 4. SEM image of the PC sample

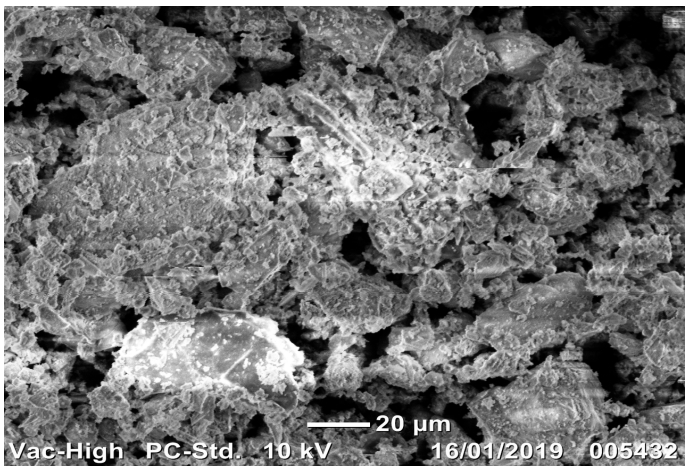

Figure 5. SEM image of the BM5 sample

Characterization by Scanning Electron Microscopy (SEM) of the samples (PC and BM5) allowed the observation of the pores of the samples and the impact of the inclusion of the date palm fibers in Portland cement on the porosity of this matrix.

Figure 4 and 5 show respectively, the images recorded by the

Scanning Electron Microscope (SEM) on samples PC and BM5.

The comparison of the two figures (4 and 5) shows the increase of the pores in the sample BM5 with respect to PC.

SEM analysis shows that strengthening portland cement with 5% date palm fibers (DPF) increases the porosity of

the matrix. The increase in porosity includes a reduction in thermal conductivity. This result is in agreement with the thematic results found previously. This explains the insulating capacity of the new prepared material.

IV. CONCLUSION

The objective of this study was to study the impact of the inclusion of date palm fibers in portland cement on the thermal and chemical properties of this matrix.
The characterization results are as follows:

- The RAMAN results have shown that DPF is well incorporated into Portland cement.
- Conductivity results confirmed the insulating power of date palm fibers.
- The inclusion of fibers (PDF) has increased the porosity of the matrix.
- The results of the Scanning Electron Microscope (SEM) reveal that thermal conductivity decreases with increasing porosity.

REFERENCES :

[1] M. Lahouioui, M. ois, L. Ibos, A. Ghorbal, Etude des performances thermiques de matériaux à matrice cimentaire renforcés par des fibres de bois de palmier traitées, 2nd Springer Euro-Mediterranean Conference for Environmental Integration (EMCEI): 10- 13 October 2016, Sousse, Tunisia (https://www.emcei.net/).

[2] N. Benmansour, B. Agoudjil, A. Boudenne, Etude des performances de produits renouvelables et locaux adaptés à l'isolation thermique dans le bâtiment, 29ème Rencontre de l'AUGC Tlemcen. (2011) pp.233–243.

[3] Chehma.A, H.F.Longo, Siboukeur.A, << Estimation du tonnage et valeurs alimentaire des sous produits du palmier dattier chez les ovins >>, Recherche Agronomique, vol.7, 2000, p.15-17.

[4] B. Agoudjil, A. Benchabane, A. Boudenne, L. Ibos, M. Fois, Renewable materials to reduce building heat loss: Characterization of date palm wood, Energy and Buildings. Vol.43 (2011) pp. 491–497. DOI:10.1016/j.enbuild.2010.10.014.

[5] A. Korjenic, V. Petránek, J. Zach, J. Hroudová, Development and performance evaluation of natural thermal-insulation materials composed of renewableresources, Energy and Buildings 43 (2011) 2518–2523.

[6] Kriker, G. Debicki, A. Bali, M.M. Khenfer, M. Chabannet, Mechanical properties of date palm fibres and concrete reinforced with date palm fibres in hot-dry climate, Cement and Concrete Composites. Vol.27 (2005) pp.554–564. DOI:10.1016/j.cemconcomp.2004.09.015.

[7] N. Benmansour, B. Agoudjil, A. Gherabli, A. Kareche, A. Boudenne, Thermal and mechanical performance of natural mortar reinforced with date palm fibers for use as insulating materials in building, Energy and Buildings. Vol.81 (2014) pp. 98–104. DOI:10.1016/j.enbuild.2014.05.032.

[8] M. Chikhi, B. Agoudjil, A. Boudenne, A. Gherabli, Experimental investigation of new biocomposite with low cost for thermal insulation, EnergyandBuildings.Vol.66(2013)pp.267–273. DOI:10.1016/j.enbuild.2013.07.019.

[9] N. Chennouf, B. Agoudjil, A. Boudenne, K. Benzarti, F. Bouras, Hygrothermal characterization of a new bio-based construction material: Concrete reinforced with date palm fibers, Construction and Building Materials.Vol.192 (2018) pp.348–356. DOI:10.1016/j.conbuildmat.2018.10.089.

[10] ISOMET 2114: 2011. Thermal properties analyzer: User's Guide, Version 120712, Applied Precision.

[11] U.P. Agarwal, Raman imaging to investigate ultrastructure and composition of plant cell walls: distribution of lignin and cellulose in black spruce wood (Picea mariana), Planta 224(5) (2006), 1141–1153.

[12] N. Gierlinger, M.Schwanninger, The potential of Raman microscopy and

Raman imaging in plant research, Spectroscopy vol. 21 (2007) pp.69–89.

[13] M. Chylińska, A. Zdunek, M. Szymanska-Chargot, Imaging of polysaccharides in the tomato cell wall with Raman microspectroscopy, Plant Methods (2014) pp.1-9. http://www.plantmethods.com/content/10/1/14

[14] B. Hasanzadeh, F. Liu, Z. Sun, Monitoring hydration of UHPC and conventional paste by quantitative analysis on Raman patterns,Construction and Building Materials. 2016, Vol 114, pp. 208-214. DOI: 10.1016/j.conbuildmat.2016.03.178

[15] S. Abani, F. Hafsi, A. Kriker, A. Bali, Valorisation of Date Palm Fibres in Sahara Constructions, Energy Procedia. Vol.74 (2015) pp.289–293. DOI:10.1016/j.egypro.2015.07.608.